Status Report on Activities in Hall A - 2000

Edited by Adam J. Sarty, Ronald D. Ransome, and Kees de Jager

January 1, 2001

Contents

1 The Facilities **5**

1.1 Optics Commissioning (Contributed by N. Liyanage) 5

1.2 Absolute Energy Measurements (Contributed by A. Saha) 6

1.3 Møller Polarimeter (Contributed by E. Chudakov) 8

1.4 The Compton polarimeter (Contributed by F. Marie) 9

1.4.1 Introduction 9

1.4.2 New technical developments 9

1.4.3 Preliminary results for E91-011 and error budget 9

1.4.4 $P_e{}^+/P_e{}^-$ determination 10

1.5 The Hall A Focal Plane Polarimeter (Contributed by S. Nanda) . . 13

1.5.1 Overview 13

1.5.2 The polarimeter 13

1.5.3 Analysis Software 15

1.5.4 Calibration Database 16

1.6 Electron Calorimeter for E99-007 (Contributed by O. Gayou) . . . 19

1.6.1 Introduction 19

1.6.2 Calorimeter Tests 20

1.6.3 Conclusion 21

1.7 The RCS Photon Spectrometer (Contributed by A. Nathan, for the RCS Collaboration) 23

1.7.1 Introduction 23

1.7.2 Photon Calorimeter 23

1.7.3 Veto Detector 28

1.7.4 Data Acquisition 29

1.8 The Hall A Photon Radiator (Contributed by R. Gilman) 32

1.8.1 Overview 32

1.8.2 The radiator 32

1.9 The Polarized ^{3}He Target (Contributed by J.-P. Chen) 34

1.10 The Cryogenic Target (contributed by J.-P. Chen) 36

1.11 Electronics Dead-Time Measurements (Contributed by. R. Michaels) 38

1.12 Analysis Software (Contributed by J.-O. Hansen) 41

1.12.1 ESPACE 41

1.12.2 The Hall A Object-Oriented Analyzer 42

1.13 Slow Controls (contributed by J. Gomez) 44

1.14 Spectrometer Alignment (contributed by J. Gomez) 44

1.15 Spectrometer Collimator Offsets (Contributed by J. LeRose) . . . 45

2 Hall A Instrumentation Upgrade for an 11 GeV beam **47**

2.1 Physics Requirements 47

2.2 The large-acceptance spectrometer 48

2.3 High Performance Electromagnetic Calorimetry 49

2.4 A ^{3}H Target 50

3 Summaries of Experimental Activities **52**
3.1 E89-019/E94-012/E99-008 52
3.2 E89-028 54
3.3 E89-044 56
3.4 E91-010 59
3.5 E91-011 63
3.6 E93-049 66
3.7 E93-050 68
3.8 E94-004 72
3.9 E94-010 73

4 References **75**

5 Members of the Hall A Collaboration **77**

6 Completed Hall A Experiments **82**

7 Hall A Publications **84**

List of Figures

1 *Beam polarization results during the E91-011 July run.* 11
2 *Energy dependence of the photon spin asymmetry for the two electron beam-helicity states.* 11
3 *Fit of* ΔP_e. 12
4 *HRS Detector stack with the FPP* 14
5 *FPP chamber 4 repair* 14
6 *CH2 Analyzer test assembly* 15
7 *Carbon Inclusive Analyzing powers* 17
8 *Hydrogen elastic peak from the hadron arm momentum-difference spectrum.* 19
9 *Results of the calorimeter test for E99-007* 22
10 *Plan view of the RCS experiment in Hall A.* 24
11 *RCS Photon Calorimeter Frame* 26
12 *Schematic of the RCS Calorimeter light monitoring system.* 27
13 *A schematic of the RCS trigger.* 30
14 *The trigger scheme for the RCS calorimeter.* 31
15 *Electronics Deadtime as function of strobe rate.* 40
16 *Lay-out of Hall A showing the configuration including the MAD spectrometer and the polarized* ^{3}*He target.* 48

17 *Photon resolution on a plot Q^2 vs. s. Contours of constant $x_{\rm Bj}$ and constant incident energy E_0 are indicated separately.* 50
18 *Comparison between G_{Ep}/G_{Mp} for the $^1H(\vec{e},e'\vec{p})$ reaction measured in E89-028 and in E93-027 (open circles) [15].* 55
19 *Preliminary results for the double ratio, $(P_T/P_L)_D/(P_T/P_L)_H$, for $^2H(\vec{e},e'\vec{p})$ to the ratio for $^1H(\vec{e},e'\vec{p})$.* 55
20 *Missing energy and momentum spectra for E89-044.* 57
21 *(a) Raw asymmetry versus data set. Solid(open) circles are from the left(right) spectrometer. The step pattern is due to the insertion of the half-wave plate. The $\chi^2 = 33.7$ for 39 degrees of freedom. b) Helicity-correlated horizontal position difference measured near the target. c) Correction to left spectrometer data due to all of the beam parameter differences.* 62
22 *Effect of event selection criteria on missing mass peak for E91-011.* 65
23 *Angular acceptance for E91-011.* 65
24 *Ratio of in-medium to free space electric and magnetic form factors of the proton in ^4He* 67
25 *VCS Analysis Plots* 69
26 *VCS cross section below pion threshold.* 70
27 *VCS differential cross section in the nucleon resonance region* . . . 71
28 *$H(\gamma^*,p)\pi^0$ virtual photo-production cross section* 71

List of Tables

1 *Summary of Recent Hall A Beam Energy measurements* 6
2 *Contributions to the systematic uncertainty of beam polarization measurements made by the Compton Polarimeter.* 10
3 *Status of some FPP experiments in Hall A.* 13
4 *Carbon Analyzing power database* 18
5 *Radiator foils, with readback voltage from the linear encoder.* . . . 33
6 *Cryotarget nominal working temperatures and pressures.* 36
7 *Surveyed Positions of Spectrometer Collimators and Sieves.* 46
8 *Instrumentation requirements for experiments needing a large acceptance detector.* 47
9 *Kinematic coverage of E94-012 measurements.* 52
10 *The perpendicular and parallel kinematics measured during the recently completed E89-044 ^3He(e,e'p) experiment.* 58
11 *Kinematics summary for E91-011.* 64

1 The Facilities

1.1 Optics Commissioning (Contributed by N. Liyanage)

The spectrometer optics data taken in December of 1999 show that the history of Q2 and Q3 magnets has a noticeable effect on optics. The most affected matrix elements were $\langle y|y\rangle$ and $\langle\delta|\theta\rangle$, which affected the transverse position and momentum resolution. The reconstruction of horizontal and vertical angles was found to be insensitive to these effects.

To eliminate the hysteresis effects on spectrometer optics, a new magnet cycling procedure was adapted for Q2 and Q3 magnets. Use of this cycling procedure ensures that the spectrometer optics properties are constant for a given momentum.

A complete calibration data set was obtained using the new cycling procedure. These data were analyzed to obtain optics data bases that cover the full momentum range of each spectrometer. These databases should cover the requirements of the future Hall A experiments that do not use the septum magnets. Future experiments need to take only a minimal optics calibration dataset to check the existing databases and to determine the detector offsets.

After the detector swap between the two spectrometers in September, 2000, optics data were obtained for both spectrometers. Analysis of these data indicates that the spectrometer optics are unaffected by the detector swap and that the existing databases can also be used with the new spectrometer configurations.

1.2 Absolute Energy Measurements (Contributed by A. Saha)

Date	Pass	ARC (MeV)	ep (MeV)	ep Strip	[(ep/Arc)-1] $\times 10^{-3}$
Dec 11, 1999	1 Pass	842.6 ± 0.2	843.1 ± 0.2	2	0.6 ± 0.4
Dec 15, 1999	5 Pass	4035.9 ± 0.8			
Feb 3, 2000	3 Pass	2906.3 ± 0.6	2902.2 ± 0.5	5	-1.4 ± 0.4
Feb 6, 2000	2 Pass	1954.8 ± 0.4	1955.6 ± 0.4	4	0.4 ± 0.4
Feb 10, 2000	2 Pass	1954.2 ± 0.4	1955.4 ± 0.4	4	0.6 ± 0.4
Feb 14, 2000	5 Pass	4806.8 ± 0.9	4807.9 ± 2.7	7	0.2 ± 0.7
Feb 20, 2000	5 Pass		4804.1 ± 3.0	7	
March 4, 2000	1 Pass	644.5 ± 0.1	644.8 ± 0.3	1	0.3 ± 0.6
March 5, 2000	2 Pass	1255.0 ± 0.2	1255.5 ± 0.3	2	0.4 ± 0.4
March 28, 2000	2 Pass	1255.3 ± 0.2	1255.3 ± 0.5	2	0 ± 0.4
April 2, 2000	5 Pass	3085.8 ± 0.6	3082.7 ± 0.3	5	-1.0 ± 0.4
May 5, 2000	4 Pass	4237.5 ± 2.0	4239.4 ± 0.3	6	0.4 ± 0.7
May 23, 2000	4 Pass	4530.6 ± 0.9	4530.3 ± 1.0	6	-0.1 ± 0.4
June 20, 2000	4 Pass	4531.0 ± 1.0	4530.0 ± 1.0	6	-0.2 ± 0.4
Oct 10, 2000	4 Pass	3170.4 ± 0.6	3165.3 ± 0.5	5	-1.6 ± 0.4
Oct 27, 2000	3 Pass	2389.0 ± 0.5	2389.4 ± 0.5	4	0.2 ± 0.4
Nov 6, 2000	4 Pass	4606.7 ± 1.5	4606.7 ± 0.6	6	0 ± 0.4

Table 1: *Summary of Recent Hall A Beam Energy measurements*

A series of systematic beam energy measurements has been performed with both the Hall A Arc-Energy method and the *ep* method. Discrepancies were surfacing at beam energies other than around 3 GeV between the two methods and this warranted a systematic check of the results. As described earlier, the Arc method uses instrumentation in the Hall A arc section (Scanners, BdL measurements of the arc dipoles etc...) developed initially by the French Collaboration (Pascal Vernin and the Saclay group). The *ep* method has been developed by the Clermont-Ferrand group of the French Collaboration (Pierre Bertin et al.,) and is a stand-alone device along the Hall A beamline located 17 meters upstream of the target.

The algorithm to determine the Hall A Arc integral in the Arc method had

an inconsistency of approximately one part in 1000, and this correction has to be applied to all previous Arc energy measurements. Moreover, the *ep* results have also to be corrected by a small amount due to a more precise determination of the *ep* target position. These corrections modify the previously reported comparisons of the Arc and *ep* methods. Table 1 reports the results of all measurements made by both methods during the past year after these corrections have been applied. Measurements taken with the same energy per pass are lumped together for the February and March 2000 runs. Both methods show good agreement with each other within their respective uncertainties except at around 3 GeV, where there seems to be a non-linearity with pass number for the *ep* method. Since for different energy ranges, different microstrip detectors are employed for the *ep* method, it seems that the knowledge of the placement of the 5th microstrip for the *ep* detector may be incorrect. This needs to be further verified with dedicated measurements and rectified in the near future.

1.3 Møller Polarimeter (Contributed by E. Chudakov)

The Hall A beam line is equipped with a Møller polarimeter, whose purpose is to measure the polarization of the electron beam delivered to the hall. During the period from 01 Oct. 1999 to 30 Sept. 2000, 28 measurements of the beam polarization were made. The systematic error of each measurement is estimated to be about 3% relative, while the statistical error is about 0.3%.

At the beginning of 2000, the three Møller polarimeter quadrupole magnets were equipped with new power supplies able to provide up to 300 A - the maximum current allowed for the magnets. The old power supplies could only provide up to 120 A. The new power supplies also considerably improved the stability of operation, since the old supplies used to trip about 2-3 times per month requiring an entry into the hall to reset them.

The beam line downstream of the Møller polarimeter has been equipped with two new quadrupole magnets providing a better possibility to use a common beam line setting for different regimes, as the regular physics running, Møller measurements and Compton polarimetry measurements.

The target foil magnetization was re-measured using a different, more reliable, technique. The new measurements found a non-uniformity of the foils used. The target polarization obtained is about 3% higher than the old value. Therefore all the beam polarizations measured so far have to be shifted by 3% downwards, relative, which is about one standard deviation of the systematic error quoted.

The Møller polarimeter spectrometer also was used to test and calibrate several detector prototypes, namely a lead glass calorimeter and a Lucite Čerenkov counter.

1.4 The Compton polarimeter (Contributed by F. Marie)

1.4.1 Introduction

This Compton polarimeter status report is dedicated to the new hardware and software developments realized in the year 2000. In 2000, the Compton polarimeter ran during the E91-011 and 99-007 experiments. The complete analysis of earlier HAPPEX runs, in addition to a preliminary analysis of the data obtained during E91-011, now allow the Compton polarimeter measurements to reach a systematic uncertainty level under 3%.

1.4.2 New technical developments

Since the end of the HAPPEX run in July, 1999, several technical improvements have been brought to the Compton polarimeter apparatus:

- The slow feedback of the magnet current in the 4 dipoles of the chicane allows a lock of the vertical position of the electron beam with respect to a nominal value. This procedure, which has been applied during the entire E91-011 run, together with the fast feedback system, limit the short and long time beam position variations to a 10 μm range.
- A fast acquisition of the electron detector together with the photon detector has been installed and allows the detection of the scattered photons and electrons at a total rate of 150 kHz at 40 μA, with a dead time of the order of 10%. With the electron detector, a complementary analyzing method with significantly different systematics sources will be theoretically available.
- Use of V-to-F to measure beam position with the BPM's instead of "borniers".
- Change of the mirrors of the Fabry-Perrot cavity in order to raise the power inside the cavity up to 1500 W.

1.4.3 Preliminary results for E91-011 and error budget

The Compton polarimeter ran during the entire data taking of E91-011. We present here preliminary results for 102 polarization runs (over 170) in July (see Fig. 1).

The main improvement of the systematics (see Table 2) since HAPPEX run is the reduction of false asymmetries due to beam position variations. This is due to the technical developments described above and also because photon polarization reversals have been made more frequently (every 2 min). We have also listed in Table 2 the errors expected after new analysis software (such as for the energy-correlated method) is implemented. Expected errors may also include, in some cases, the residual uncertainty after correction (run by run) of the effect.

Error sources	Present [%]	Expected [%]
Analyzing power		
Resolution & Threshold	1.9	1.0
ADC Pill up	0.5	0.1
ADC linearity	0.5	0.2
Calibration	1.0	0.3
Laser beam		
Polarization	1.0	1.0
Experimental asymmetry		
Beam positions	0.5	0.1
Background	0.3	0.2
Dead time	0.2	0.1
total	**2.6**	**1.5**
Statistic (in 30 min)	**1**	**0.7**

Table 2: *Contributions to the systematic uncertainty of beam polarization measurements made by the Compton Polarimeter.*

Statistics have been also improved, mainly due to the increase of the nominal beam energy of E91-011 compared to HAPPEX, and better stability of the beam parameters. Typically a 1% relative statistical precision has been achieved in 30 minutes.

1.4.4 $P_e{}^+/P_e{}^-$ determination

As a consequence of photon polarization reversals, one can theoretically determine separately the right and left electron polarization. One needs to calculate the experimental asymmetry A^+ and A^- between 2 photon reversals for each electron helicity state. The following relation gives the difference of polarization in absolute value for the two helicity states ΔP_e:

$$\frac{A^+ + A^-}{2} =< A_{th} > P_\gamma \Delta P_e + Fa_{R/L}$$

The problem is that the false asymmetry $Fa_{R/L}$ is of the same order of magnitude as the theoretical asymmetry $< A_{th} >$. But, if we use the energy dependence of the asymmetry $A(k)$ (see Fig. 2), taking advantage of the fact that $Fa_{R/L}$ does not depend on the photon energy, one can easily separate a constant and an asymmetry-dependent term (see Fig. 3). The preliminary analysis shows (and this is the first experimental proof at Jefferson Lab) an agreement between the two electron helicity states at the level of 1.5% during 10 minutes.

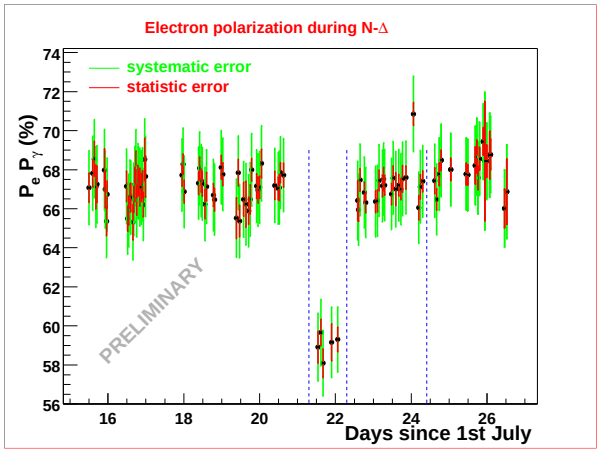

Figure 1: *Beam polarization results during the E91-011 July run. Plotted errors are for statistics and preliminary systematics evaluations. The decrease of the polarization around day 22 corresponds to a spot move of the laser at the electron beam source.*

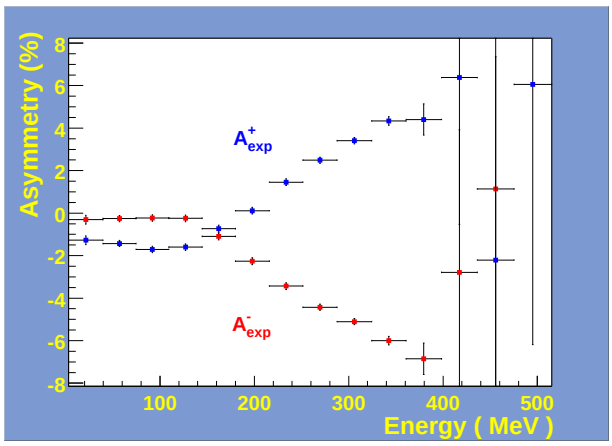

Figure 2: *Energy dependence of the photon spin asymmetry for the two electron beam-helicity states.*

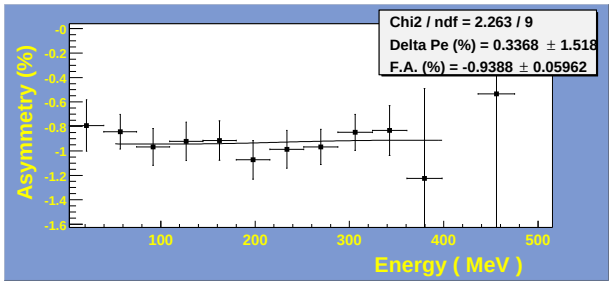

Figure 3: *Fit of* ΔP_e.

1.5 The Hall A Focal Plane Polarimeter (Contributed by S. Nanda)

1.5.1 Overview

A large number of the experiments in Hall A measure recoil proton polarization. Two polarimeter experiments so far have results that are among the most interesting findings from Jefferson Lab to date. First, Exp. 93-027 determined that the distributions of charge and magnetization in the proton are different. Second, Exp. 89-019 determined that the induced polarization in deuteron photodisintegration vanishes, giving no indication of strong nucleon-resonance contributions generally expected in meson-baryon models. A list of experiments using the polarimeter is given in Table 3 - this list does not include experiments that are yet to be scheduled. Although publications are not yet available for most of the experiments, almost all have presented invited talks at international conferences.

Experiment	Contact Person	Run Ended	Status/Publications
89-033	C. Glashausser	Aug. 1997	S. Malov *et al.*, Phys. Rev. C, in press
93-027	C.F. Perdrisat	Aug. 1998	M. Jones *et al.*, Phys. Rev. Lett. **84**, 1398 (2000)
89-028	P. Ulmer	Aug. 1999	analysis underway
89-019	R. Gilman	Nov. 1999	K. Wijesooriya *et al.*, submitted to Phys. Rev. Lett.
94-012	R. Gilman	Nov. 1999	analysis underway
93-049	R. Ent	May 2000	analysis underway
91-011	A. Sarty	Jul. 2000	analysis underway
99-007	C.F. Perdrisat	Dec. 2000	

Table 3: *Status of some FPP experiments in Hall A.*

1.5.2 The polarimeter

Transverse polarization of the proton leads to an azimuthal asymmetry in scattering from an analyzer. The Focal Plane Polarimeter in the hadron HRS measures this asymmetry from which the transverse components of the polarization in the focal plane are extracted with Fourier analysis. Knowledge of the spin transfer matrix of the spectrometer is used to trace the focal plane polarizations back to the target.

The polarimeter consists of straw tube drift chambers that determine the trajectory of incident and scattered protons from a graphite or polyethylene analyzer. There are four chambers with about 5000 wires. A schematic layout of the FPP

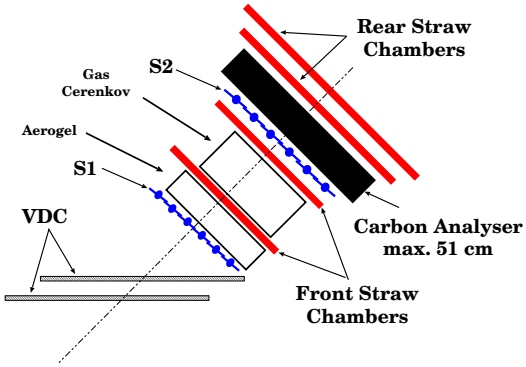

Figure 4: *HRS Detector stack with the FPP*

is shown in Fig. 4. The chambers are operated at a positive high voltage of about 1900 V with a constant flow of 68% argon and 32% ethane gas mixture. A detailed description of the polarimeter and its performance is in preparation for publication [9]. Online documentation is available at http://www.jlab.org/∼malov/fpp_home/fpp_home.html and http://www.jlab.org/∼gilman/fpp-homepage.html.

The polarimeter hardware has been largely stable since it was first incorporated into the hadron detector stack at the end of 1996. The positioning of the graphite anayzer has been incorporated into the Hall A EPICS control system. Maintenance the wire chambers and gas handling system is performed annually.

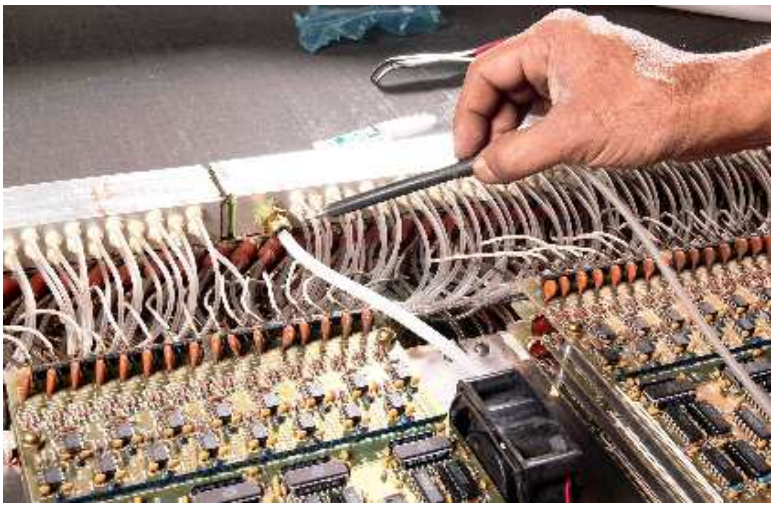

Figure 5: *FPP chamber 4 repair*

The larger rear chambers developed several gas leaks during the course of

operation. The supply gas flow rates were boosted accordingly in order to maintain detection efficiencies for each wire plane at an acceptable level. The flammable gas level sensor in the Hadron spectrometer showed a corresponding increase in the ethane level in the shield house. Several trips of the sensor alarm (above the 10% LEL setting for ethane) were observed. Most of these trips were however, were caused by helium contamination in the hall and unrelated to ethane buildup in the shield house.

During the summer 2000 shutdown, the chambers were taken out of the detector stack and leak-checked with helium by Rutgers collaborators R. Gilman, R. Ransome, and G. Kumbartzki. The leaks appear to be primarily due to dislocation of the small feed tubes to the individual straws shown in Fig. 5. A number of such well-localized leaks were repaired bringing down the leak rates of the chambers to acceptable levels. For the longer term, plans to refurbish the gas supply of the rear chambers or to switch to a non-flammable gas mixture are under evaluation.

A new CH_2 analyzer with an improved figure of merit for higher energy protons was developed and coordinated by C. Perdrisat. Installation of the CH_2 analyzer was tested during the last shutdown (See Fig. 6). The first use of the analyzer was for Exp. 99-007 during Nov.-Dec., 2000.

Figure 6: *CH2 Analyzer test assembly*

1.5.3 Analysis Software

Online data acquisition software has also largely remained stable over the past few years. The major improvement is the "straw efficiency" replay, set up by M. Jones following up on work done by E. Brash, which analyzes a large number of events to determine the wire by wire efficiency of the straw chambers. At this point, the

group has not made an effort to adapt this FORTRAN code to C++ so that it can be used under ROOT, which is expected to replace ESPACE as the Hall A analyzer in the next one to two years.

Offline analysis software has undergone several improvements. A variety of alignment and tracking algorithms are available, from E. Brash, M. Jones, K. Wijesooriya, and S. Malov. In addition to naive central-ray spin transport and full dipole spin transport, a more general spin transport code directed at *ep* elastic scattering was written by G. Queḿeńer. S. Strauch further generalized it to allow all six proton polarization components (three induced plus three polarization transfer) to be determined from the data.

The new code takes full advantage of the variation of the proton spin precession across the spectrometer's acceptance; in different parts of the focal plane different linear combinations of the proton's spin components contribute to the azimuthal distributions after the carbon analyzer. These azimuthal distributions are used to estimate the three induced and three transferred polarization components. The estimate is based on the Maximum Likelihood method. Additional constraints, such as the normal component of the transferred polarization being zero in two body reactions, may be used within the code to improve the estimates.

These more general spin transport codes both use COSY spin matrix elements to model the spectrometer, as COSY appears to provide a better description of spectrometer optical properties than other codes, such as SNAKE or TRANSPORT.

1.5.4 Calibration Database

There is now a large data base of analyzing power and efficiency measurements. The carbon inclusive analying powers are generally in good agreement with previous measurements of Los Alamos [10] and Saclay [11]. As an example, analyzing powers are shown in Fig. 7 as a function of proton kinetic energy, averaged over a polar scattering angular range of 5° to 20°. The solid triangles are previous measurements of McNaughton [10] and the squares are the measurements with the Hall A FPP.

The geometry of the Hall A polarimeter allows for much larger polar scattering angle coverage than previous polarimeters. This can be exploited at higher proton energies to obtain a better overall figure of merit. Calibration data for both the traditional 5-20° and the wider 3-70° acceptances are given in Table 4.

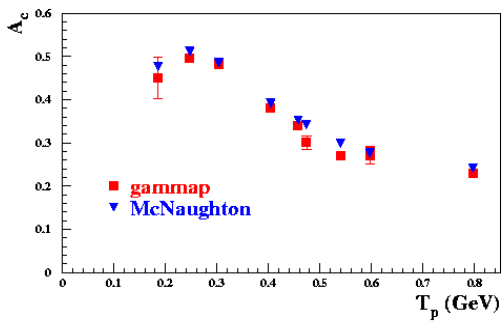

Figure 7: *Carbon Inclusive Analyzing powers from the 1999 "gammap" experiments compared to the results of McNaughton [10].*

Table 4: *Carbon Analyzing power database*

Proton	Carbon	$5^\circ \leq \theta_c \leq 20^\circ$		$3^\circ \leq \theta_c \leq 70^\circ$		
Momentum (MeV/c)	thickness (cm)	A_c	eff. (%)	A_c	eff. (%)	$\mu G_e/G_m$
594	3.81	0.375 ±0.059	2.9	0.198±0.063	7.6	0.930 ± 0.067
619	3.81	0.394 ±0.044	2.5	0.225±0.050	5.8	0.910 ± 0.061
658	7.62	0.345 ±0.023	4.7	0.141±0.032	14.8	0.961 ± 0.033
725	7.62	0.501 ±0.021	3.7	0.265±0.026	8.7	0.952 ± 0.034
750	11.43	0.508 ± 0.010		0.259±0.013	8.7	0.966 ± 0.022
765	11.43	0.481 ± 0.023	5.33	0.259±0.020	14.7	0.933± 0.026
815	11.43	0.471 ± 0.025	5.5	0.249±0.031	12.9	0.959 ± .039
961	19.05	0.389 ± 0.019	8.2	0.236±0.021	17.1	0.966 ± .033
984	22.86	0.364 ± 0.006		0.220±0.007	20.0	0.950 ± 0.015
1037	22.86	0.344 ± 0.016	10.1	0.226±0.018	20.4	0.865 ± .029
1056	22.86	0.302 ± 0.049	13.8	0.213±0.048	27.6	0.923 ± .086
1142	26.67	0.287 ± 0.021	16.8	0.209±0.020	33.8	0.900 ± .038
1148	34.29	0.298±0.011	12.97	0.219±0.009	27.5	0.848±0.018
1216	34.29	0.268 ± 0.016	12.7	0.205±0.015	23.8	0.825 ± .027
1251	34.29	0.245 ± 0.027	15.0	0.192±0.025	28.4	0.851 ± .050
1260	41.91			0.190±0.008	25.0	0.869 ± 0.014
1452	41.91			0.211±0.021	25.0	0.798 ± 0.033
1460	49.53	.230 ± 0.040	23.5	0.198±0.034	43.8	0.733 ± .058
1547	45.72	0.216±0.0121	16.50	0.185±0.010	34.3	0.753±0.015
1626	49.53	0.166 ± 0.087	17.1	0.143±0.073	32.2	0.816 ± .115
1638	49.53	0.198 ± 0.027		0.172±0.023	30.0	0.728 ± 0.026
1698	49.53			0.160±0.030	28.0	0.720 ± 0.031
2053	49.53			0.126±0.022	31.0	0.726 ± 0.027
2341	49.53			0.095±0.017	32.0	0.612 ± 0.032
2623	49.53	0.100 ± 0.019		0.078±0.017	32.0	0.609 ± 0.047

1.6 Electron Calorimeter for E99-007 (Contributed by O. Gayou)

1.6.1 Introduction

The precision of the measurement of the ratio ${G^p}_E/{G^p}_M$ at $Q^2 = 5.6$ GeV^2 with a beam energy of 5.7 GeV (Nov.-Dec., 2000) can be improved if the solid angle of the electron detector is matched to that of the recoil proton detector. This solid angle matching cannot be achieved with the HRS. At the kinematics of experiment E99-007, the electron scattering angle is larger than the proton recoil angle; therefore the Jacobian for the electron is larger than one, and the solid angle for the electron detector must be twice as large as that of the proton detector.

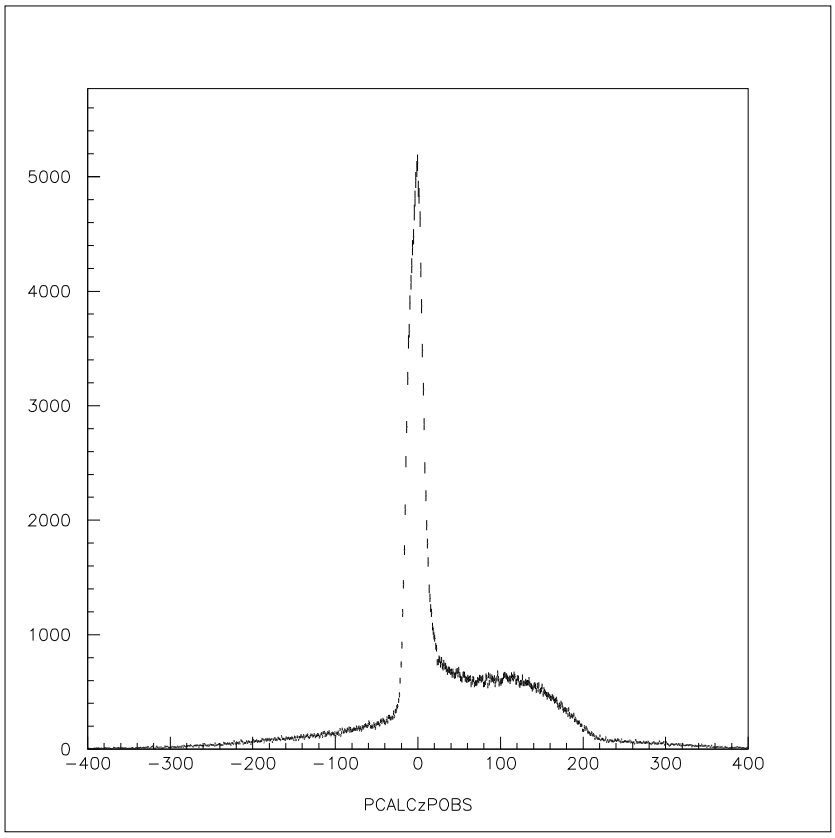

Figure 8: *Hydrogen elastic peak from the hadron arm momentum-difference spectrum. See text for details.*

Figure 8 illustrates the necessity of detecting the electron in coincidence. It shows the momentum-difference spectrum (in MeV/c) between the *calculated* proton momentum from the observed scattering angle assuming the event was elastic, and the *observed* proton momentum. The elastic events are under the peak cen-

tered at 0. A simple cut on this spectrum is not sufficient to separate elastic events from accidentals and target-wall contamination in a clean way.

We have adopted the technique of using a calorimeter made of lead-glass blocks to detect the electron. We tested this technique in the spring, 2000, using forty-five 15×15 cm^2 blocks (most of them coming from the pion rejector) in an array of 5 (horizontal) $\times$ 9 (vertical). The test had 2 purposes: to check the validity of the method by measuring the ratio G_{E_p}/G_{M_p} at $Q^2 = 3.0$ GeV^2 and comparing it with the published result of E93-027, and to measure the background radiation from the beam dump and the target walls.

1.6.2 Calorimeter Tests

The blocks had a 15×15 cm^2 cross section and were 30 or 35 cm long. The Čerenkov light was detected by XP2050 photomultipliers and the signal was sent to LeCroy 1881 ADC's. The standard deviation for the position resolution of the detector was approximately $15/\sqrt{12} = 4.3$ cm when the position is defined by one block only. For about 30% of the events, the resolution was improved by taking into account the energy deposited in the neighboring blocks.

During the test conducted in May, 2000, the beam energy was 3.395 GeV, with a current of 50 μA. The calorimeter was placed at an angle of 41° at 8 m from the target. The data acquisition was triggered by an event in the right HRS (proton side), set at 30°.

The results are shown in Fig. 9. To evaluate the usefulness of TOF information, 2 blocks in the middle of the calorimeter were connected to TDC's (LeCroy 1875). The first row of the figure shows that the use of TDC's is of considerable help in reconstructing clusters, i.e. including only the blocks that have been hit by the electron, and eliminating random hits on the left of the elastic peak in the left-most plot (about 4 times as many as in the elastic peak). On the right-most figure of this row, elastic events are under the peak at 1800 MeV. The events to the left of the elastic peak are in part from the radiative tail, in part from spill-over of showers in the neighboring blocks, which need to be included in the cluster.

The middle row of Fig. 9 shows $E_{miss} = E_{beam} + M_p - E_p - E_{calo}$. Elastic events are under the peak at $E_{miss} = 0$. The right-most figure shows the peak when cuts are applied on both the hadron-side elastic peak and on the angular correlation. The angular correlation cut is made on the diagonal of the first 2 plots of the last row in the figure.

We collected data with an empty cell to study background in the Hall, mostly from the beam dump. We saw almost no signal in the calorimeter, probably because the HRS that was between the detector and the beam dump offered very good shielding. Beam was then sent onto the dummy target, so that the contribution of the target walls could be estimated: it was found to be of the order of 10^{-4} under the elastic peak, as shown in the last plot of Fig. 9. We also measured accidentals by delaying the ADC gate during a LH2 run; no accidentals

were present in the elastic peak.

1.6.3 Conclusion

The test has shown that the use of a simple calorimeter made of large blocks is sufficient to obtain a clean separation of elastic events from background radiation, covering a large solid angle at high luminosity. The ratio ${G^p}_E/{G^p}_M$ at 3.0 GeV^2 was measured to be 0.62 ± 0.048, to be compared with the result of E93-027, 0.61 ± 0.032 (uncertainties are statistical only). A calorimeter of similar design was assembled for use in E99-007, using blocks from the pion rejector and from the shower counter of the right HRS (electron side), with a total of 147 blocks read by both ADC's and TDC's.

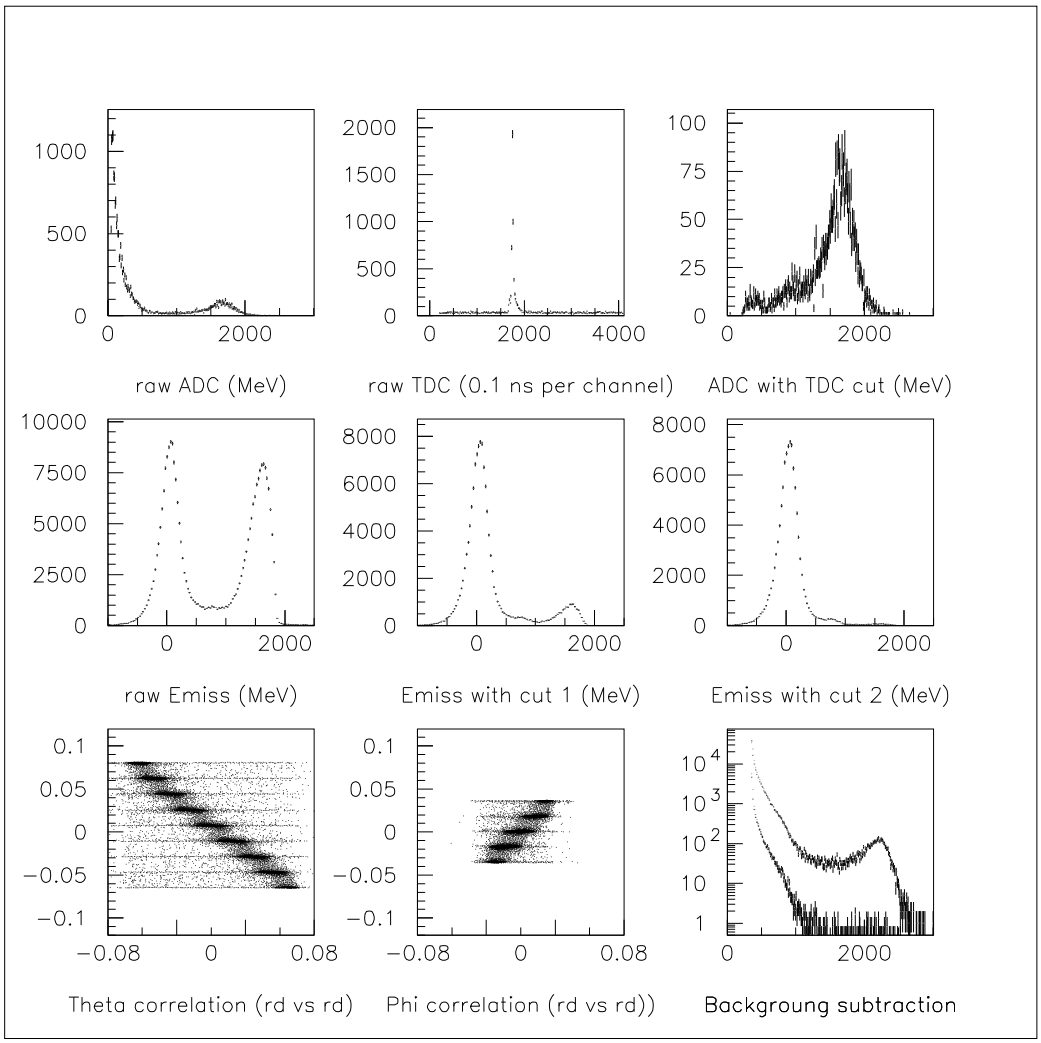

Figure 9: *Results of the calorimeter test for E99-007. From left to right:* **Row 1:** *raw ADC spectrum for one lead-glass block; raw TDC spectrum for the same block; same ADC spectrum after cut on elastic peak in TDC;* **Row 2:** E_{miss}*-spectrum for all events;* E_{miss}*-spectrum after cut on the elastic peak in the HRS focal plane (not shown here);* E_{miss}*-spectrum with additional cut on the* θ *and* ϕ *ep angular correlation; the elastic peak now stands alone;* **Row 3:** θ_e*-*θ_p *angular correlation, all events;* ϕ_e*-*ϕ_p *angular correlation, all events; raw ADC spectrum, LH2 and empty target for one block.*

1.7 The RCS Photon Spectrometer (Contributed by A. Nathan, for the RCS Collaboration)

1.7.1 Introduction

The Real Compton Scattering experiment (E99-114) will measure the differential cross section for Compton scattering from the proton at incident photon energies between 3 and 6 GeV and over a wide range of CM scattering angles. A high duty factor electron beam with current ≥ 10 μA is incident on a 6% copper radiator located just upstream of the scattering target. The mixed beam of electrons and bremsstrahlung photons is incident on a 15-cm LH_2 target. The experimental layout is shown schematically in Fig. 10. For incident photons near the bremsstrahlung endpoint, the recoil proton and scattered photon are detected with high angular precision in a magnetic spectrometer and photon spectrometer, respectively. The magnetic spectrometer is one of the pair of High Resolution Spectrometers (HRS) that are part of the standard Hall A equipment. The cryogenic hydrogen target and bremsstrahlung radiator to be used are also part of the standard Hall A equipment. The photon spectrometer is a new piece of equipment which is being constructed for this experiment. It consists of a large-area, highly segmented calorimeter of lead glass (Section 1.7.2), a segmented veto detector (Section 1.7.3), and a deflection magnet. The complexity of this "third-arm" detector required a completely new data acquisition system (Section 1.7.4).

1.7.2 Photon Calorimeter

The principal detector in the photon spectrometer is a lead glass calorimeter (see Fig. 11), which is used to measure the energy and angle of the scattered photon.

During the 1998 and 1999 test runs, a calorimeter prototype - containing 25 (5×5) lead glass modules - was installed and tested under actual experimental conditions. An energy resolution better than $\sigma_{\delta E/E} = 1\% + 6\%/\sqrt{E}$ and a spatial resolution of 4.3 mm was achieved with the prototype. Other results, including studies of luminosity limitations, gain stability, algorithms for calorimeter calibration and position resolution optimization, etc., are addressed in the 1998 and 1999 *RCS Internal Reports* and *Status Report on Activities in Hall A — 1999*.

During the last year the following progress was achieved in development and construction of the photon calorimeter:

— More than 720 detector modules have been assembled and 704 of them have been installed in the detector;

— Cooling system and cable communication have been developed;

— The calorimeter modules gain-monitoring system has been developed.

The calorimeter consists of 32 layers, each having 22 lead glass modules — 704 modules in total. In Fig. 11 two views of the assembled calorimeter with the frame

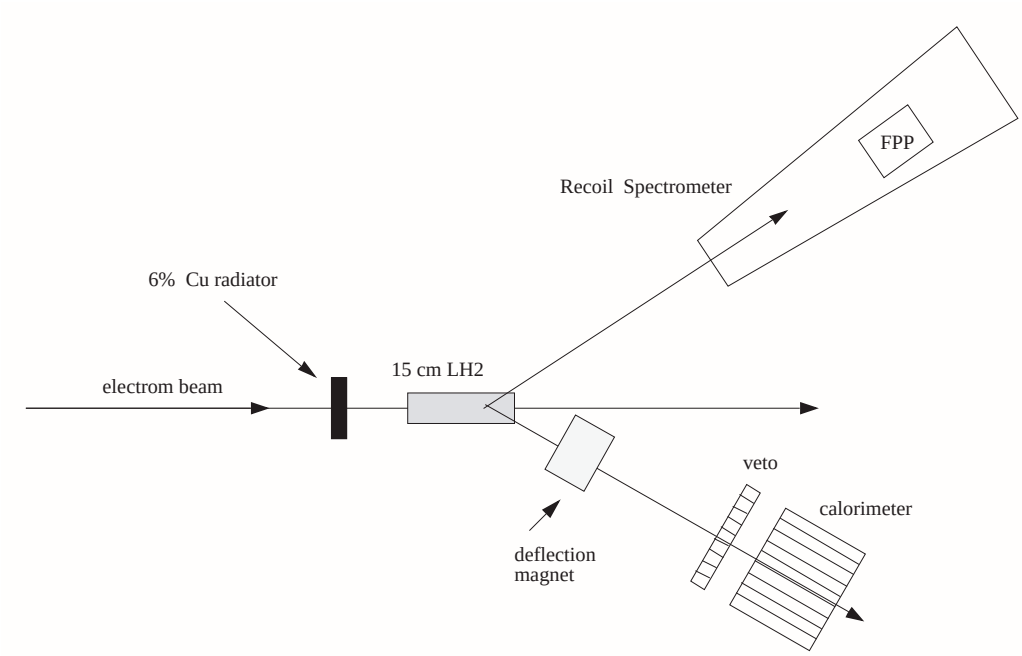

Figure 10: *Plan view of the RCS experiment in Hall A.*

are shown. The frame has been designed for 88×128 cm^2 acceptance (22×32 blocks), with possibility to extend the acceptance up to 104×144 cm^2 (26×36 blocks).

Each calorimeter module is a $4 \times 4 \times 40$ cm^3 lead glass of type TF–1. Čerenkov light produced by interacting photons and electrons in the lead glass is measured by a 34 mm diameter photomultiplier of type FEU-84-3. Optical coupling between the lead glass and PMT is made using BC-630 optical grease. The PMT is pressed to the lead glass with a 5 kg permanent force applied along the PMT axis. Stability of this kind of optical coupling was checked during one week of tests in 70° C temperature. The performance of each PMT and HV divider was also tested.

Cooling of photomultipliers and bases is accomplished using forced airflow through the PMT housings. A system of 176 outgoing 1/4 inch diameter tubes was constructed with an airflow of 0.5 l/s in each individual tube. The PMTs and bases are thus kept at a temperature of $37\ ^\circ\ C$.

Cooling and cabling patch panels are mounted on eleven swinging supports, which allows convenient access to the PMT housings for installation and repairing.

A light monitoring system was developed for gain measurement of each calorimeter element during the experiment. A schematic of the monitoring system is shown in Fig. 12. UV light pulses 5 ns long from a nitrogen laser are directed to a plastic

scintillator producing blue light pulses. The light from the scintillator is sent by a set of plastic fibers to a Lucite plate installed in front of the lead glass array. The light scattered from the plate and detected by the calorimeter PMTs is used for gain monitoring. The stability of the system is being studied.

All high voltage crates have been installed and tested. The crates have remote control, and are controlled by Java software. A system of cabling for application of HV is under construction.

All work on the photon calorimeter development is done in the Test Lab at JLab.

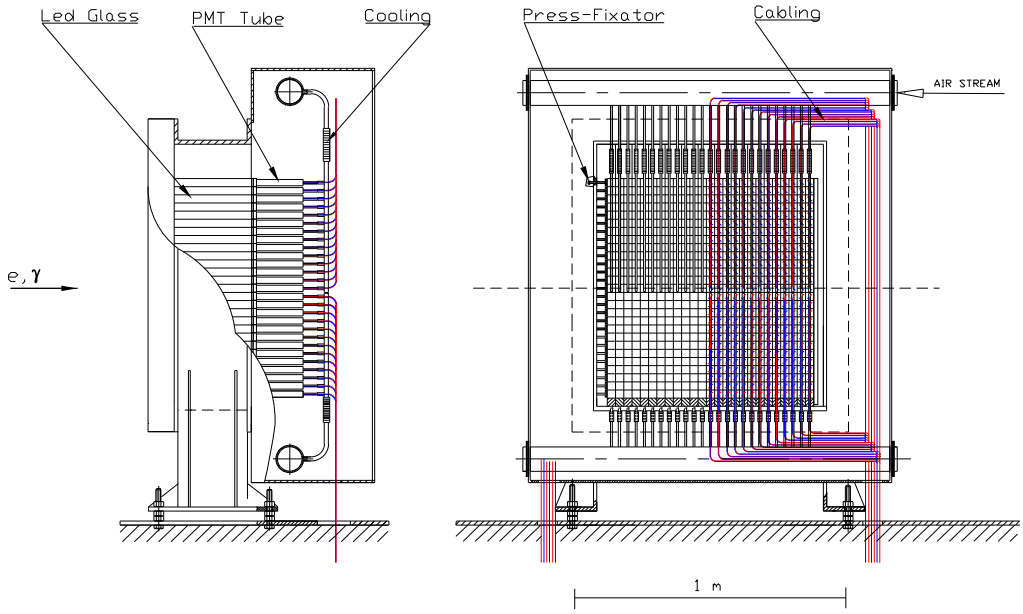

a) b)

Figure 11: *Side view — (a), and front view — (b) of the RCS Photon Calorimeter frame.*

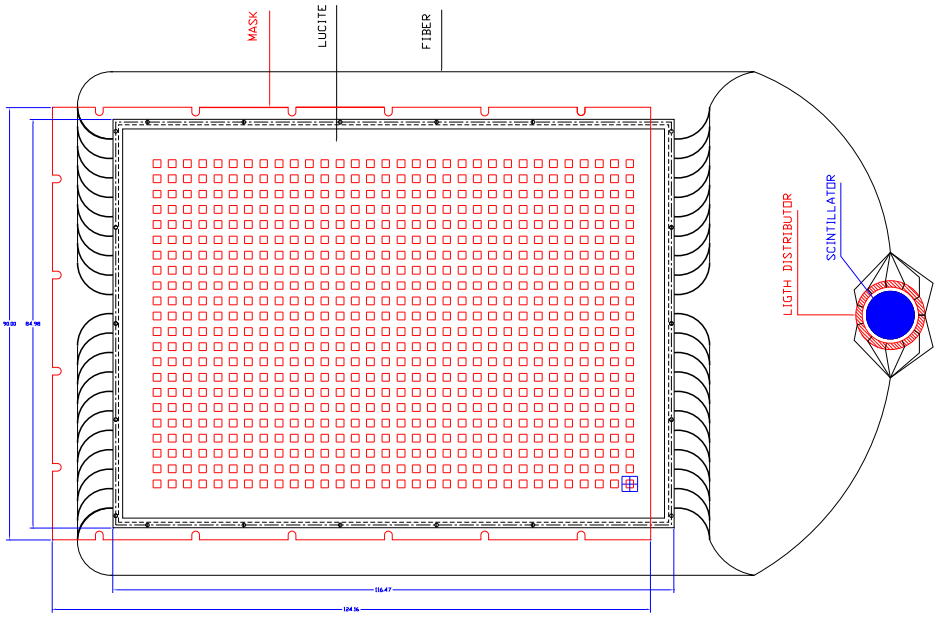

Figure 12: *Schematic of the RCS Calorimeter light monitoring system.*

1.7.3 Veto Detector

Because the RCS experiment uses a mixed beam of bremsstrahlung photons and electrons, and because the kinematics of *ep* elastic scattering is essentially identical to that of RCS, it is necessary to provide some means of identifying charged particles in the photon detector. Consequently, the RCS experiment will utilize a charged-particle veto detector consisting of two planes of detectors (vertical and horizontal) placed just in front of the calorimeter. Feasibility studies utilizing both parasitic and dedicated beam time have shown that the counting rates in the veto will be large, so that it is necessary to segment the detectors to keep the rate in any given detector less than about 1 MHz. The segmentation also allows for spatial correlations between the veto and calorimeter. Multi-hit TDC's will be used to improve the veto efficiency at high counting rates. Although the total rate in each plane of veto counters will be high, demanding a spatially correlated coincidence between the two planes reduces the accidental-veto probability to an acceptably small level.

Each plane of the detector consists of two rows of solid ultra-violet transmitting (UVT) Plexiglas (acrylic) radiators in a geometry that matches the acceptance of the calorimeter (1.28 m vertical by 0.88 m horizontal). There are a total of 216 detectors. Each of the 128 horizontal detectors is 44 cm long, and each of the 88 vertical detectors is 64 cm long; all detectors are 2 cm wide by 2 cm thick. A Čerenkov detector was chosen over the more standard plastic scintillator because extensive studies have shown that this reduces the background counting rate in the high-radiation background of Hall A by at least a factor of two. Each detector is viewed by a single PMT of type XP2972. The low light output of the detectors necessitates the use of an amplifier. We are utilizing a design of the JLab detector group (V. Popov) that incorporates an amplifier directly in the voltage divider, without the need for any additional power supply beyond the high voltage. Each detector is coupled to an optical fiber, which will ultimately be tied in to the same gain monitoring system that will be used for the calorimeter.

The design and construction of the detector, including the mechanical frame onto which the detectors are mounted, have been taking place at the University of Illinois since January, 2000. All the parts constructed at Illinois are complete and have been delivered to JLab for assembly in the Test Lab. The voltage dividers/amplifiers are under construction by Photonis and will be delivered by the end of 2000.

1.7.4 Data Acquisition

The data acquisition system of the RCS experiment utilizes the standard HRS readout package and a separate Photon-Arm readout package. This Photon-Arm readout package is newly built and is designed especially for reading out data from the Photon-Arm – including the calorimeter, the veto counter, and possibly a MWPC. A standard Hall-A Trigger Supervisor is installed on the Photon-Arm to coordinate the event readout from the photon arm and the hadron arm and to provide the gate signals. When running in the stand-alone mode, the Trigger Supervisor serves as gate provider, event prescaler, and scaler counter. The main electronics for digitizing the data are the LeCroy FASTBUS 1800 series modules. The readout controller of the Photon-Arm is a MVME Single Board CPU mounted in the SFI FASTBUS-VME interface. The analog signals from each of the calorimeter blocks (704 blocks total) and the veto counter (216 channels total) are sent to the FASTBUS ADCs and the hit pulses on the veto counters are sent to the multihit FASTBUS TDCs. The hit pulses of the summed signals from the calorimeter are sent to the ADC and TDC also. The MWPC will only be used during the position calibration and the readout will utilize CAMAC electronics.

The hadron trigger from the S0 scintillator counter and the photon trigger from the calorimeter are sent to the Photon-Arm electronics logic and are ultimately fed into the Trigger Supervisor. The timing relation of both triggers is carefully measured and the signals are properly delayed so that a coincidence event will generate a coincidence trigger. The coincidence window is determined by the width of the hadron trigger pulse and is set to 100 ns. The width of the photon trigger pulse is set to 10 ns so that the coincidence events are synchronized with the photon trigger. Upon receiving a trigger signal, the Trigger Supervisor will issue a Level 1 Accept (L1A) signal, which is used to gate the ADCs and to stop the TDCs in the photon and hadron arms. This is illustrated in Fig. 13.

The photon trigger is provided by the calorimeter. The RCS calorimeter has 22 x 32 blocks; the signals from every 2 x 4 array of blocks, except the outermost layer of blocks, are first summed by a custom-made linear-summing module. Then four of the summed signals from the 2 x 4 array are summed again to form a signal summed over 32 blocks. This arrangement provides sufficient overlap so that events occurring at the boundaries of the blocks are included in the trigger. The scheme is illustrated in Fig. 14. The signals from the sum of 32 blocks forms a master OR, the output of which gives the photon trigger.

The construction of the RCS DAQ began in September, 1999. The setup is located in the Test Lab and utilizes a Linux PC platform to run the control software (CODA). Most of the electronics and cables have been installed and the system has been tested under stand-alone condition since May, 2000. The system has been utilized to diagnose various parts of the photon-arm detector package. It is expected that the system will move into Hall-A during the shutdown in the spring of 2001, and subsequently test the full system with the HRS readout.

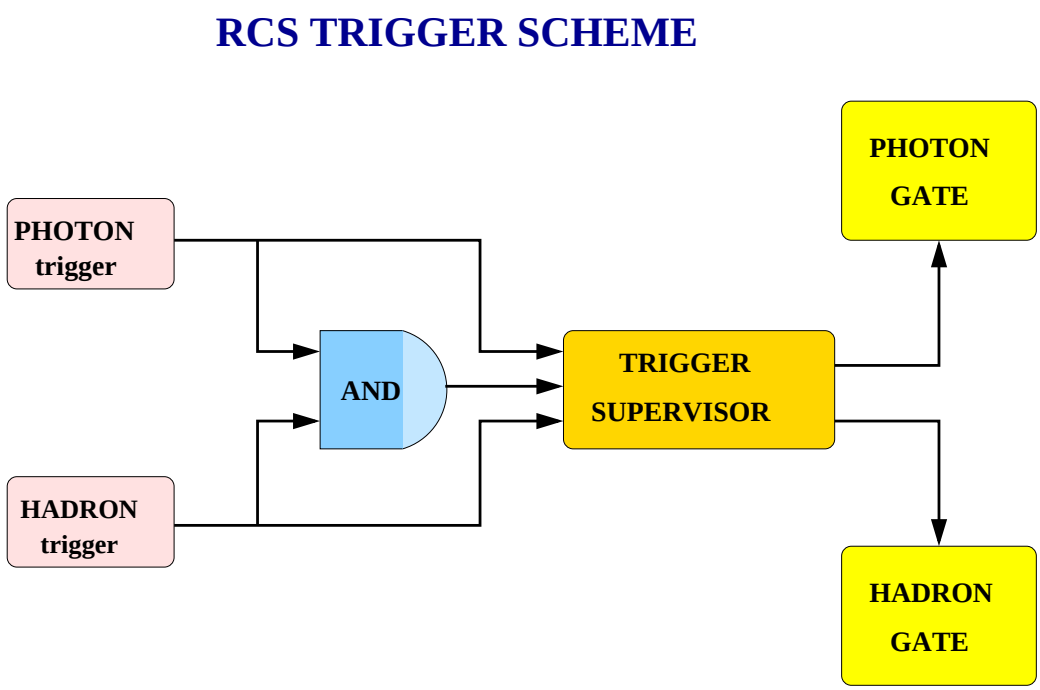

Figure 13: *A schematic of the RCS trigger.*

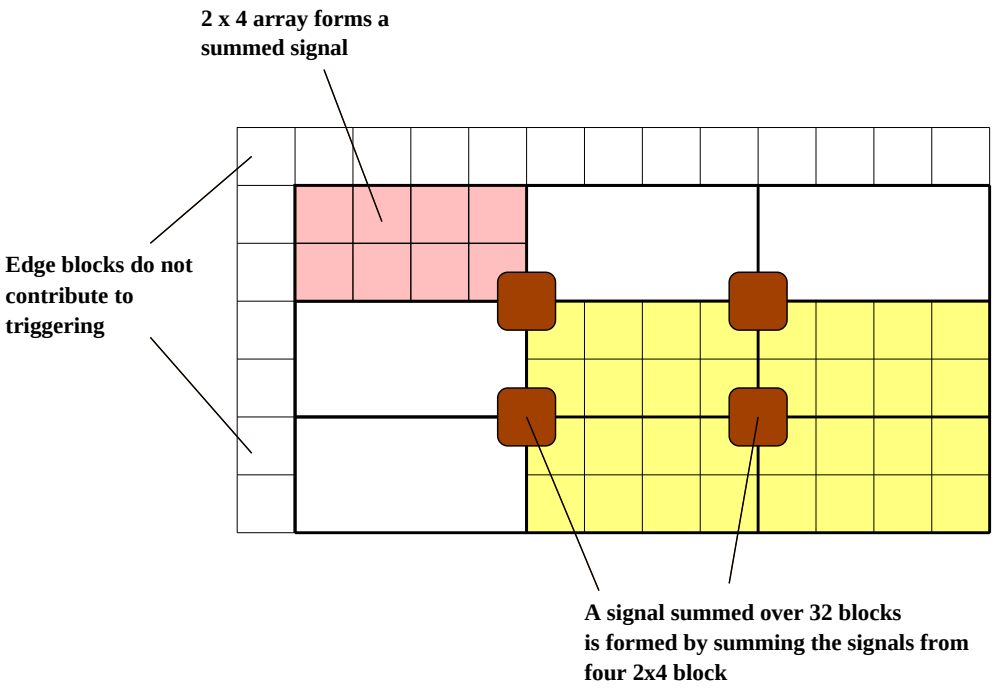

Figure 14: *The trigger scheme for the RCS calorimeter.*

1.8 The Hall A Photon Radiator (Contributed by R. Gilman)

1.8.1 Overview

There exists a number of real photon experiments in Hall A, studying real Compton Scattering (E99-114), deuteron photodisintegration (E89-019*, E99-008*, E00-007, E00-107), and pion production (E94-012*, E94-104). (Note: The * marks experiments that have already successfully taken data with the radiator.) Real photons are produced through bremsstrahlung radiation in a thin copper foil upstream of the main target. There is no chicane nor radiator dump currently in Hall A, so both the photon and electron beams interact with the target, and the photo- and electro- reactions must be separated.

1.8.2 The radiator

The radiator consists of a U-shaped frame with 5 positions in which foils are mounted - this allows the radiator to be moved when beam is on. In general, the radiator is blocked at the *out* limit when not in use. There is no reason to set the radiator to the *in* limit. People wanting to use the radiator should coordinate with Ed Folts to ensure that the radiator, and its associated water cooler, are hooked up, along with the cooler FSDs. The control box power supplies also need to be turned on, and the radiator unblocked. After use, the power should be turned off, and the radiator should be blocked off again. Disconnecting the water cooler and FSDs should be done by Hall A staff coordinating with accelerator staff.

The radiator can be operated with either manual or remote controls; the manual control system used a function generator borrowed from, and returned to, the polarized $^3\vec{He}$ target group. The remote controls were written by Dave Wetherholt, and are operated by phoning MCC with your request. The controls can be brought up from the main Monticello EPICS GUI, and monitored in the counting house. The manual controls were used for the first set of experiments; the remote controls have now been tested - though not with the radiator under vacuum - and will be used for future experiments.

At the start of an experiment, the radiator foil positions should be calibrated. Table 5 shows approximate information, which should not change greatly, but needs to be verified. (Note: initially the radiator was mounted above the beamline; it is now mounted below the beamline so as not to interfere with the LVDT positioning system. Since the beam is not exactly centered in the beamline, there will be some offset.) The voltage readback values assume a 5.02 V supply.

The position calibration procedure is to move the radiator, while monitoring the ion chamber readbacks. A 5 μA unrastered beam should be used. Ion chamber levels will be large when the beam hits the foils, but small in the gap between the foils. The size of the gap corresponds to a range of about 0.03 to 0.04 V in the readback. The center of the foils can be determined by finding the gaps between foils 2/3, 3/4, 4/5, and 5/6. The calibration needs to be coordinated with Dave

Wetherholt; only he can adjust the foil positions in the software.

Position	Thickness (% L_{rad})	Readback Voltage (V)
out limit	-	0.15
1	(no foil)	0.51
2	2.04	1.35
3	3.06	2.19
4	4.08	3.03
5	5.10	3.87
6	6.12	4.70

Table 5: *Radiator foils, with readback voltage from the linear encoder.*

More information about the radiator can be found in web pages maintained by R. Gilman; see
http://www.jlab.org/~gilman/gammap99.

1.9 The Polarized ^{3}He Target (Contributed by J.-P. Chen)

The Hall A polarized ^{3}He target [1] uses optically pumped Rubidium vapor to polarize ^{3}He nuclei via spin exchange. It has been successfully used for the first round of experiments E94-010 [2] and E95-001 [3]. The target polarization was monitored with NMR using Adiabatic Fast Passage (AFP). NMR AFP measurements on water and Electron-Paramagnetic-Resonance (EPR) measurements were used calibrate to the ^{3}He NMR signal. The NMR water calibration analysis was reported in last year's status report. The EPR analysis was completed this year. The result was reported in a student thesis [4]. The final calibration constants from the NMR water calibration and from the EPR analysis are $\kappa_{water} = 5.67 \times 10^{-4}(1 \pm 2.3\%)$ (mV/%/amgats/cm^2), and $\kappa_{EPR} = 5.56 \times 10^{-4}(1 \pm 2.4\%)$ (mV/%/amgats/cm^2). They agree with each other very well. The final error on the polarization measurement is $\sim 4\%$, of which the largest contribution comes from the uncertainty in the target density. Often, as in the GDH experiment (E94-010), the physics quantity goes into the spin structure functions (g_1 and g_2) and the extended GDH sum is the product of the target polarization and the target density. This product has a smaller error of $\sim 3\%$ since the contribution of the target density in the product cancels the density contribution in the target polarization determination.

A third independent check was performed by measuring the elastic scattering asymmetry. The ratio of the measured asymmetry to the world data gives a measure of the product of the beam polarization and the target polarization. The deduced target polarization is in excellent agreement with the NMR water and EPR results. The difference is $\sim 2\% \pm 5\%$.

The polarized target has been set up in the target lab in the EEL building. The NMR system has been completely checked out and is fully functional. A number of water calibrations were performed, and were consistent with the results obtained during the first round of experiments. EPR system was also set up. The first EPR signal was seen recently. A number of tests are still ongoing to fully debug the system, and improvements are being considered. One attractive option is to continuously monitor the target polarization with EPR, which will require additional testing and work. We are still studying the feasibility of such an option.

Most of the surviving target cells have been re-characterized: their maximum polarization and lifetime were re-measured. At least one 40 cm and two 25 cm cells are good cells (have good polarizations and lifetimes). The Princeton/UVa group (G. Cates) is continuing to produce cells until the setup is moved to the University of Virginia (mid-Oct.). At least one good 40 cm cell with very good lifetime has been produced. Once the setup is moved to UVa, it will be immediately set up to resume cell production. In the meantime, the William & Mary group (T. Averett) has started to produce cells with help of a glass blower at UVa. The first cell was produced in October, 2000, and ruptured before it was tested. A second cell was also produced in October, and will be in November, 2000. The effort will continue with a goal of producing at least 5 each of good 40 cm and 25 cm cells for the two

planned experiments in 2001 (E99-117 and E97-113).

We plan to have six new 30 W diode lasers for the optical pumping, along with several used ones as spares. There are only two new ones now. Since the vendor who supplied the current 30 W diode lasers has stopped producing lasers at this wavelength, we have switched to a new vendor (Coherent). A new demo laser from Coherent has been tested at JLab. The new laser works very well. With small modification of the optics, the new laser can be mixed in with the old lasers. Four more new lasers will be purchased shortly by JLab (2), U. Kentucky (1) and U. Virginia (1).

Design has started to accommodate the new kinematics requirements as well as to add new features and improvements. The Helmholtz coil mount will be re-designed to provide rotation capability. There will be a new motion subsystem and improved target ladder subsystem. The reference cell mount and coupling will be re-designed. New RTD mount and wire harness will be available for reliable monitoring of the target temperature. Other improvements include a correction to the laser hut and an improvement for easy alignment.

The target control system is going through a transition. The EPICS control software developed by the polarized ^{3}He collaboration for the last round of experiments will become the responsibility of the JLab EPICS group. New improvements will also be developed by the EPICS group with help from the polarized ^{3}He collaboration. The temperature readout part has been worked on. Work on all the other parts are just starting. The new tasks include the new motion system control, the new laser system control and the two way communications between EPICS and LabView, which is used for the target polarimetry.

1.10 The Cryogenic Target (contributed by J.-P. Chen)

The Hall A cryotarget system [5] consists of 3 loops: loop 1 for gaseous helium (either ^{3}He or ^{4}He), loop 2 liquid hydrogen and loop 3 liquid deuterium. The nominal operation conditions are summarized in Table 6.

Target	T [K]	P [psi]	ρ [(g/cm^3)]	length [cm]
LH_2	19	26	0.0712	15, 4
LD_2	22	22	0.162	15, 4
^{3}He	6	200	0.081	10
^{4}He	6	220	0.144	10

Table 6: *Nominal working temperatures and pressures. The target densities and lengths are listed too.*

The liquid hydrogen and deuterium loops have already been successfully used in a number of experiments. The helium loop was installed and commissioned during the period covered by this report.

The helium cryotarget was installed in November-December, 1999. A new ^{3}He gas handling system was constructed and tested. About 3700 liters of ^{3}He gas were taken over from Bates, which filled loop 1 to about 110 psi at 6.3K. When Hall C is not using its ^{3}He target, their ^{3}He gas supply can be combined with the Hall A supply, and there then should be enough ^{3}He gas to fill to above 200 psi at 6K. During the initial helium target cool-down test there was a loop fan failure. All three loop fans were replaced to have the correct type of fans. They have been working fine since then. The helium target was then successfully commissioned. The density fluctuation with beam current was studied to be about a few percent at less than 100 μA with a nominal loop fan speed (60 Hz) [6]. During the commissioning, it was discovered that the coolant flow was limited by the pipe size of the heat exchanger. The heat exchanger was designed for the liquid hydrogen/deuterium target which uses the '15 K' coolant. The 15 K coolant has a pressure drop of 13 atm. The 1/4" size pipe of the heat exchange is not a limitation for the coolant flow in this case. However, the helium target uses the '5 K' coolant which has a pressure drop of less than 2 atm. With such a small pressure drop, the heat exchange pipe became the limiting factor for the coolant flow. With this limitation, the total available cooling power was only about 220 W. During the January, 2000, maintenance period, the helium cryotarget was reconfigured to use two (both loop 1 and loop 3) heat exchanges in parallel to increase (double) the cooling power for helium target. This arrangement was temporary since it used up two loops, making the deuterium loop unavailable for experiments.

The helium target was then successfully used for two experiments, E89-044 (^{3}He) and E93-049 (^{4}He) with maximum cooling power up to about 440 W.

The target change from liquid hydrogen to liquid deuterium or vice versa is relatively fast (5 minutes). However, since the helium target uses 5 K coolant

while the liquid hydrogen and deuterium targets use 15 K coolant, the change-over would take about 16 hours.

During the August/September, 2000, maintenance period, a new heat exchanger with proper pipe size for the helium loop was installed in loop 1. The loop 3 heat exchanger has been re-connected to the deuterium target. Noisy high power heater power supplies were replaced. A number of old temperature sensors were replaced. Some pressure transducers were re-calibrated. A new optics target (a stack of ^{12}C foils) was installed in the old 10 cm dummy target location. The 10 cm dummy target was moved to the original 4 cm dummy target position and the 4 cm dummy target was removed from the target ladder and will not be available for experiments (with special request, it can be re-installed). A helium-cooled lead target was installed with coolant supply coming from the loop 3 (deuterium loop) coolant supply. The hydrogen and deuterium storage/recovery tanks were relocated from Hall A to a gas shed outside the hall.

The coolant control J-T valves have both manual (in the counting house and in Hall A) and computer control. Currently only the manual control works.

Due to the limited supply of the "beer cans" used for the liquid hydrogen and deuterium cells, and due to the experimental requirements of reduced multiple scattering after the main interaction, replacement of the beer-can cells with improved machined cells has been under study. One option is the design by the cryotarget group which has been installed in Hall C. We are waiting for the Hall C performance to see if it is a suitable solution for us. Another option is the design by the Cal State LA group which is mostly focussed on reducing multiple scattering. Prototype cells were made and study is still underway.

1.11 Electronics Dead-Time Measurements (Contributed by. R. Michaels)

Several of the experiments in Hall A aim to measure a cross section to at least 3% accuracy and need to know the absolute efficiency of the apparatus. Much of the running in Hall A has seen very high rates approaching 1 MHz in the scintillators, even if the trigger cleaned this up to a much lower rate, and therefore the electronics dead-time correction can become comparable to the required accuracy. Up until summer of 2000 we did not measure the electronics dead-time directly. This report discusses the following issues: 1) The proposed measurement scheme to be fully implemented in early 2001; 2) Results from a partial scheme which was installed during the E91-011 experiment and is being upgraded between experiments; 3) Implications for earlier experiments; and 4) Plans to reduce the dead-time.

The principle behind the measurement is as follows: we send a well-defined, recognizable pulse into the front-end of the trigger and see if it makes it through to the trigger supervisor, which is the point at which the DAQ is triggered. Also, if the DAQ is alive, the trigger supervisor will accept this pulser trigger and it will show up in the datastream as a tagged event. The fraction of such events that get lost is the dead-time correction. Note, one can measure both the electronics and the DAQ dead-time separately this way.

There are two spectrometers in hall A whose scintillator trigger systems are nearly identical. In each, there are two planes of scintillators, called S1 and S2. Each plane is divided into six scintillator paddles which have a phototube (PMT) on either end. The trigger first forms the logical "and" between the left and right PMTs of paddles. These coincidences clean up some noise. The results are then used to form a coincidence of the S1 and S2 planes in a memory lookup unit (MLU). Triggers typically involve paddle N in S1 matching the same paddle number (N) in S2. This description is not complete but is sufficient to understand the dead-time measurement.

To measure the dead-time we will send a signal into the four PMTs required to make a trigger (left and right on one paddle in S1 and S2). Each paddle will have its dead-time measured in turn, i.e. we first pulse paddle 1, then paddle 2, etc., up to 6. The pulser will be sent to a TDC as a flag, and also the "and" of the pulser and trigger will be sent to scalers to measure the dead-time directly. The rate of pulsing an individual paddle will be about 1 Hz and will be proportional to beam current. The pulser signals will be coupled to the PMTs using linear fan-in circuits which preserve the resolution and low-noise of the apparatus.

The scheme described above is the full system covering the entire focal plane which we plan to install in early 2001. Another method to study the dead-time that will be implemented as soon as possible will be to send signals from various stages of the trigger to multi-hit TDCs and analyze the losses in a sample of "minimum bias" triggers. This can help us locate the bottlenecks in the system;

a suspected but unproven bottleneck is the first MLU.

During the summer of 2000, we partially implemented the pulser scheme, involving only one scintillator paddle. Analysis from Mark Jones of the data from the E91-011 experiment is shown in Fig. 15. The electronics dead-time (EDT) is plotted against the sum of the strobe rates on the two spectrometers. The motivation for such a plot is that we expected the strobing of the MLU to be the main source of EDT. Evidently the EDT depends on other experimental conditions in a way still to be determined. A detailed report on the EDT during E91-011 is available from Mark Jones (see www.jlab.org/~jones/e91011/report_on_deadtime.ps). During the September shutdown, the system was upgraded so that two paddles are pulsed, with the pulses timed to follow the hadron momentum, allowing the EDT to be measured separately in each spectrometer in scalers – although at the moment, one must use TDC information to decide which pulsed paddle made the trigger. The full focal plane measurement system described above will involve custom electronics being built by the JLab electronics group.

For prior experiments, there were no direct measurements of the EDT. One possible way to recover is to parameterize the EDT in terms of the rates on the scintillators, which have always been measured, using present and future EDT measurements. Also the "I scans", which study the flatness of the cross section as beam current is increased, are useful, especially using a target like ^{12}C which does not boil. Finally, all experiments have large samples of loose triggers which only require the "or" of S1 and S2 planes which appear to show dead-time effects.

The dead-time slope in Fig. 15 is approximately 200 ns, and one can expect to build a trigger with much less dead-time. A simple improvement planned for Fall of 2000 is to install "width adjustor" modules which will allow us to have narrow ($\leq$ 40 ns) signals throughout the trigger, while sending wider signals (100 ns) to the digital delays. Currently our signal widths are 100 nsbecause of the requirement of these delays. Another possibility being explored is to replace the MLUs with simple overlap logic electronics; however, proof that this will be helpful requires an analysis of the bottlenecks, which we hope to obtain from "minimum bias" triggers as described above. We should also compare the dead-time of the MLU in transparent versus strobed modes, either using beam or a high-rate random pulser during a shutdown.

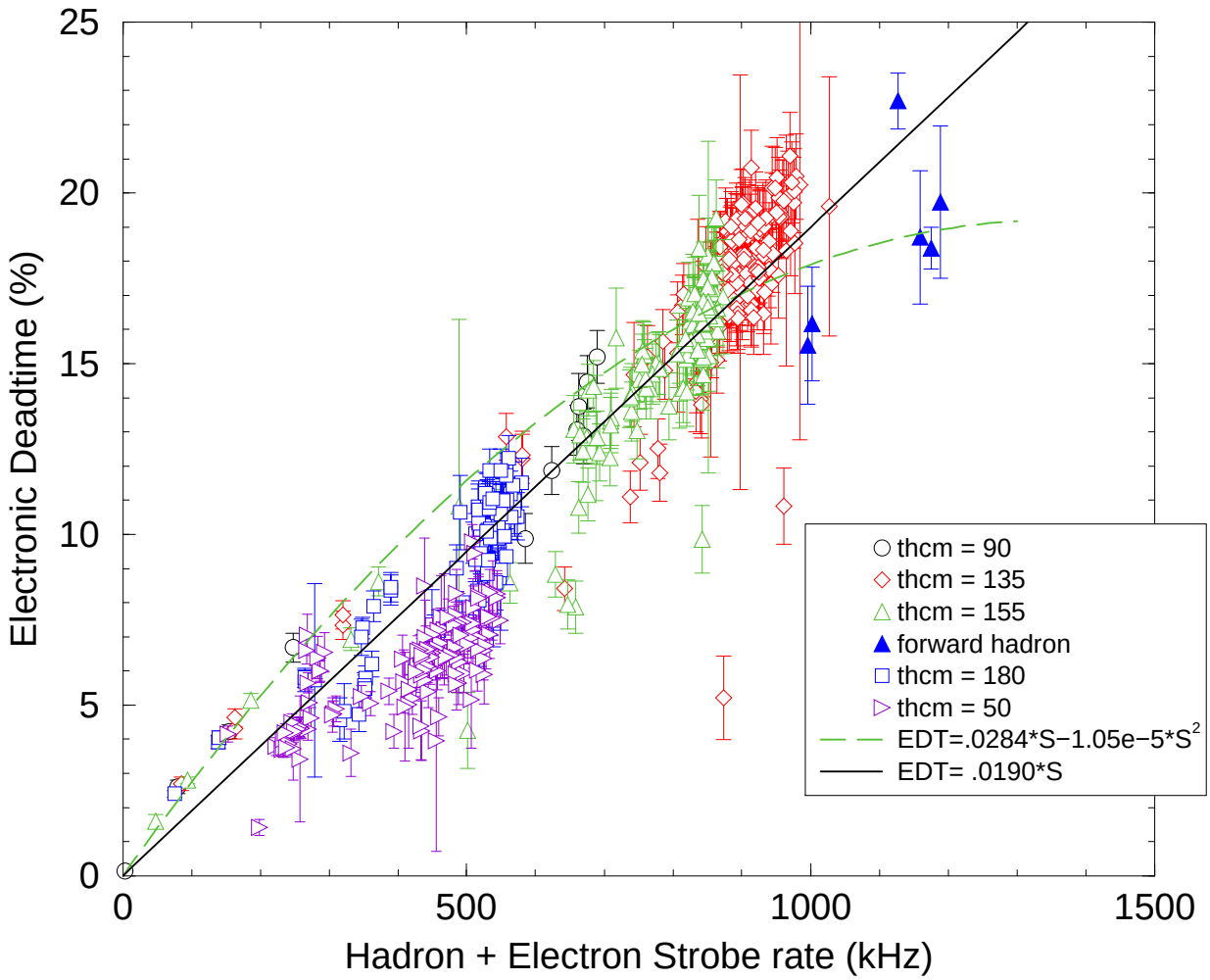

Figure 15: *Electronics dead-time (%) versus the sum of strobe rates on two spectrometers for coincidence triggers during E91-011 experiment in summer 2000. Notice that the X-axis extends to about 1 MHz. Figure from Mark Jones; see full report at www.jlab.org/~jones/e91011/report_on_deadtime.ps*

1.12 Analysis Software (Contributed by J.-O. Hansen)

1.12.1 ESPACE

Over the last year, the changes to the Hall A analysis program ESPACE have been relatively minor. This has been mainly due to the fact that recent experiments have had little need for new functionality in ESPACE, but also indicates that the program is stable and mature. Upcoming experiments for fall/winter 2000, and spring 2001, are likely to change this as detector relocations and additions will place stronger demands on the analysis software.

Since October, 1999, three new official versions of ESPACE have been released:

- With version 2.8.0 (3 Nov 1999), improvements to the β and coincidence ToF calculations were added, contributed by Nilanga Liyanage, and ROC15 was included to support `2daq` running mode (two independent DAQs, one for each spectrometer).

  Further, ESPACE can now be compiled with three different preallocated memory sizes: "lite", "medium", and "large", where "large" corresponds to the allocation of earlier program versions. The "large" configuration consumes about 50MB of virtual memory, which is not always practical with laptops, heavily loaded, or older computers. The "medium" and "lite" models require only about 20MB and 12MB, respectively. Of course, the smaller configurations do not allow definition of as many histograms and logical tests as the large configuration.

  In addition, a number of small convenience changes were made.

- For version 2.8.1 (26 Jan 2000), full support for RedHat Linux 6.x was added, and the Makefiles were improved to require less manual configuration. The Makefiles now attempt to determine automatically the required Fortran run-time library on Linux. In addition, the static linking of the executable is now the default on Linux, which improves portability between the many available versions and distributions of Linux whose shared library configurations are not necessarily compatible with each other.

  Along with these improvements of ESPACE, we had to compile CERNLIB 99 for RedHat 6.x ourselves because the official version from CERN was incompatible with ESPACE/RH6. This allowed ESPACE to run on RH6 for the first time. As of spring 2000, the Computer Center supports a RedHat 6.x version of CERNLIB 2000, which should be used for compiling ESPACE.

- In version 2.8.2 (12 Mar 2000), minor changes were made to improve compatibility with different versions of Linux.

Version 2.9 of ESPACE is currently in preparation and will be released in October, 2000. It will include support for a new BPM readout scheme and various other maintenance improvements.

1.12.2 The Hall A Object-Oriented Analyzer

An effort is underway in Hall A to write a new analysis package using object-oriented programming implemented in C++. This program will eventually replace ESPACE. The new analyzer is based on the ROOT system [7,8], an object-oriented framework that has been under development at CERN since 1995 and has been adopted by several major collaborations at FNAL, BNL, and elsewhere. Since many physics-specific capabilities (e.g. histogramming, data structure I/O) have already been implemented in ROOT, they do not have to be reinvented for our purposes; and since ROOT is widely used elsewhere, a large code base as well as support is readily available.

The chief goal in designing the new analyzer has been flexibility and maintainability of the code in an environment where frequent changes of the experimental configuration (detector components, entire spectrometers) occur. To this end, detectors and apparatuses (collections of detectors, e.g. a spectrometer) are defined as classes that are derived from abstract Detector and Apparatus base classes. More specialized Detectors and Apparatuses can either be constructed by inheritance from the generic Detector and Apparatus objects which are provided with the core analyzer package, or by writing a new class which inherits directly from the abstract base class. All classes specific to an experiment are included into the analyzer by dynamic loading of shared libraries. As a result, neither the code base nor the libraries and executable of the core analyzer require any modifications to accommodate a new experiment; all experiment-specific code is contained in separate classes and shared libraries.

To communicate results, Detector and Apparatus objects can define "global variables", which are accessible by symbolic names and are managed by a singleton class that contains a hash list of the names. Access to such global data is by read-only pointer, so the name needs to be resolved only once, the data are always current, and no copying is required.

Steering of the analysis is done through CINT, the interactive C/C++ interpreter that is part of ROOT. The main advantages of using CINT are direct interactive access to all defined classes and easy compilation of analysis scripts. Scripts are written in C++, although in-depth knowledge of C++ is not necessary to write basic analysis scripts. Unlike other ROOT-based analysis packages, the event loop of the Hall A analyzer is not implemented as a CINT script (although it could) but as a precompiled class (Analyzer). To modify the analysis flow and parameters, various member functions can be called on this class. Experiments requiring special analysis usually will write their own Analyzer as a class derived from the standard Analyzer.

The standard Analyzer implements a three-step analysis chain. In the first step, a method called `Decode()` is executed on each defined Detector object. `Decode()` performs any operations on detector data that can be carried out without knowledge of the data from any other detectors. This includes retrieving raw

data from the event buffer and scaling them to physically meaningful values, for instance photoelectrons or drift times. In the second step, `Reconstruct()` is called for each defined Apparatus. This function carries out any computations that require knowledge of data from other detectors within the Apparatus, for example fitting of tracks through several drift chamber planes using calorimeter clusters for further guidance, or reconstruction of target quantities. Finally, in the third step, the information from all Apparatuses is combined. This typically involves computation of physics quantities such as missing energy and relative coincidence time. The third step is implemented in a special "Physics" class. Several standard Physics classes are provided by the core analyzer package, for instance for (e, e') and $(e, e'p)$ reactions. Experiments can either extend these existing classes or define a completely new one.

At the end of each analysis step, an optional set of logical tests can be executed, and further processing of the current event can be terminated if certain conditions are not satisfied. Additionally, sets of histograms can be filled. Tests and histograms can be defined on the fly, i.e. without requiring any program compilation. This is functionally similar to the COOLHANDS package used in ESPACE. Tests and histograms are typically defined in plain-text files which are read from the CINT steering script before the start of the analysis. The expression parser for the test and histogramming classes allows processing of complex arithmetic formulae, transcendental functions, etc. The parser class directly inherits from the ROOT `TFormula` class.

The format of the analyzer output can be defined in a special "event" class. Different Event classes may be defined for an experiment, for instance one class for online analysis that contains mostly raw detector data and diagnostic information and another for offline analysis containing mostly physics quantities. The Event object that is desired for an analysis is defined in the steering script, and a pointer to it is passed to the Analyzer. For each event, a method called `Fill()` is executed on the currently defined Event class. `Fill()` typically copies data from "global variables" of interest to member variables of Event. Typically, the output consists of a ROOT tree, but can also be a more simple structure.

The implementation of the object-oriented analyzer is in progress at the time of this writing. Preliminary tests without any track reconstruction but with significant detector analysis give a very reasonable processing speed of 500-1000 events/s on a 500MHz Linux PC, indicating that a speed comparable to that of ESPACE will probably be achieved in the end.

Up-to-date information about this project can be found on the Web at `http://hallaweb.jlab.org/root`.

1.13 Slow Controls (contributed by J. Gomez)

The main effort during the last year went into transferring the Hall A slow controls to the Accelerator Controls Group (ACG) as agreed about one and a half years ago. Under this agreement, ACG will maintain and upgrade existing Hall A systems, as well as develop any new application which may be required.

Initial progress was slow. Basically, it took longer than expected to:

- get fully operational the agreed upon EPICS version (3.13) at which the transfer was going to take place.
- develop new EPICS drivers for Hall A devices conforming to both ACG standards and the 3.13 version of EPICS.

At this point, however, a major set of device drivers has been completed and tested. Transfer of the signal databases is also proceeding well. Most of the present/future changes described below should be invisible to the users. The present status/plans are:

- Three Input/Output Controllers (IOCs) have been completely transferred to ACG: hallasc17 (gas shed), hallasc4 (hadron detectors), and hallasc11 (electron detectors).
- An IOC has been established for handling the gas system of the RICH counter under construction.
- Transfer of the drivers and signal databases for hallasc5 (beam current monitors) is nearing completion. It is expected that by the end of calendar 2000, both hallasc5 and hallasc9 (Hall A cryogenics monitoring) will be transferred to ACG.
- Hall A controls-related displays are being redone following the standard ACG display hierarchy. This change should facilitate problem reporting by both Hall A users as well as Machine Control Center (MCC) operators to the ACG on-call software person. Swap between the presently used displays and the new set should take place in the beginning of 2001, along with the installation of a dedicated file server for controls.

1.14 Spectrometer Alignment (contributed by J. Gomez)

The displacement gauge system (so called Linear Variable Differential Transformer - LVDT system) continued being used for spectrometer pointing, while another attempt was made to make operational the cable extension encoders. Based on previous inspection/tests of the cable extension encoders themselves, several problems were identified:

- the encoder support platform of each spectrometer (two encoders per platform) does not have vertical compliance to compensate for vertical misalignments caused by either mechanical installation or spectrometer vertical motion.
- mounting of each encoder on its support platform does not have any horizontal compliance to compensate for mechanical errors like the actual distance between the ring and the encoders.
- "walk" of the encoder steel cables on the central aluminum ring relatively shallow (45°) V-groove walls.

The first two problems manifest themselves as grooves (1 - 2 mm deep) cut into the guiding bushing of the encoders, which quickly reduce their useful life. Their solution requires substantial engineering work since one has to provide freedom of rotation (translation) around (along) several axes while keeping minimal coupling among axes. The third problem is believed to be the cause of the erratic behavior of the encoders. It is also related to the first problem. Since the encoder support platform of each spectrometer does not have vertical compliance, the encoder cables are pushed up/down the V-groove walls when they are not aligned to the center of their corresponding groove. One possible solution has already been mentioned above, another is to reduce the coefficient of friction between the steel cables and the aluminum ring. We attempted this second solution. A Teflon coating was applied to the grooves of the ring, but the system still could not be made to work reliably.

Alternative ways to measure the spectrometer angle/pointing have been discussed with JLab's survey group. We lean towards using a method similar to the one used to set the spectrometer angle except that one makes use of a "scale" located at the central ring below the target. Ways to implement the "scale" and "reading" method are being evaluated and the viability of some of the proposed methods is been tested.

Finally, during the August/September shutdown, the spectrometers were surveyed to check the location of the slits with respect to the spectrometer optical axis. Tests were also carried out to determine the influence of spectrometer vacuum on slit location.

1.15 Spectrometer Collimator Offsets (Contributed by J. LeRose)

During August and September of 2000, the survey group at JLab remeasured the positions of the collimators and sieves in both spectrometers. The formal reports from the survey group are: JLab Alignment Group DT #'s: A627 & A629. The results are shown below in Table 7) . For a more detailed discussion of the results see http://hallaweb.jlab.org/news/minutes/sieves_2000.htm.

	Δx (mm)	Δy (mm)	z (mm)
Right (formerly Hadron) Sieve	0.92	-1.46	1175.5
Right Large Collimator	2.44	-0.17	1101.0
Left (formerly Electron) Sieve	-0.38	3.46	1184.3
Left Large Collimator	-1.86	4.06	1109.9

Table 7: *Surveyed Positions of Spectrometer Collimators and Sieves.* Δx *is the horizontal displacement of the Sieve or Collimator from its ideal position.* $+x$ *is to the left when facing the spectrometer.* Δy *is the vertical displacement of the Sieve or Collimator from its ideal position.* $+y$ *is up.* z *is the distance from the ideal target position to the sieve or collimator.*

2 Hall A Instrumentation Upgrade for an 11 GeV beam

2.1 Physics Requirements

With the 12 GeV upgrade (11 GeV for Halls A, B and C) a large kinematic domain becomes available for studies of deep inelastic scattering. The combination of high luminosity and high polarization of beam and targets will place Jefferson Lab in a unique position to make significant contributions to the understanding of nucleon and nuclear structure and of the strong interaction in the high-x region. Precision data are scarce in this region (especially for the spin-dependent nucleon structure), due to the fact that the quark distribution drops rapidly when x becomes large. Table 8 lists the physics requirements of a number of experiments which need a large acceptance spectrometer, mainly in the high-x region.

Nr.	Exp.	P_{max} [GeV/c]	Angle acc. [msr]	Mom. acc. %	Mom. res. %	Hor. ang. res. [mrad]	Vert. ang. res. [mrad]	Min. angle [degrees]
1	^{3}H/^{3}He	6	15-30	30	0.3	1	3	15-30
2	A_1^n, $g_1{}^n$	5-7	15-30	30	0.3	2	3	15-30
3	g_2^n	5	20-30	30	0.3	2	3	15-25
4	A_1^p, $g_1{}^p$	5-7	15-30	30	0.3	2	3	15-30
5	DIS-PV	6	30	30	0.3	1	3	15-25
6	semi-π	6-7	10-30	30	0.3	2	3	12-15
7	semi-K	6-7	10-30	30	0.3	2	3	12-15
8	charm	6.5	30	30	0.3	1	2	12-15
9	b_1	6	15-30	30	0.3	1	3	20-30
10	recoil p	5-7	10-30	30	0.3	1	3	15-25

Table 8: *Instrumentation requirements for experiments needing a large acceptance detector.*

In the first listed example [12], unpolarized inclusive electron scattering on ^{3}H and ^{3}He will provide precision measurements of the down quark to up quark ratio at high x. The present knowledge of this ratio, extracted from F_2 data on the deuteron, is severely hampered by the sizable corrections for Fermi motion and binding effects. The proposed data will decrease the uncertainty in the d/u ratio by an order of magnitude at large x.

In the second experiment, the spin structure functions g_1 and A_1 of the neutron will be measured accurately by using a polarized ^{3}He target. It will unambiguously establish the trend of A_1^n as x goes to 1, which will provide a benchmark test of pQCD and constituent quark models. Equivalent measurements for the proton

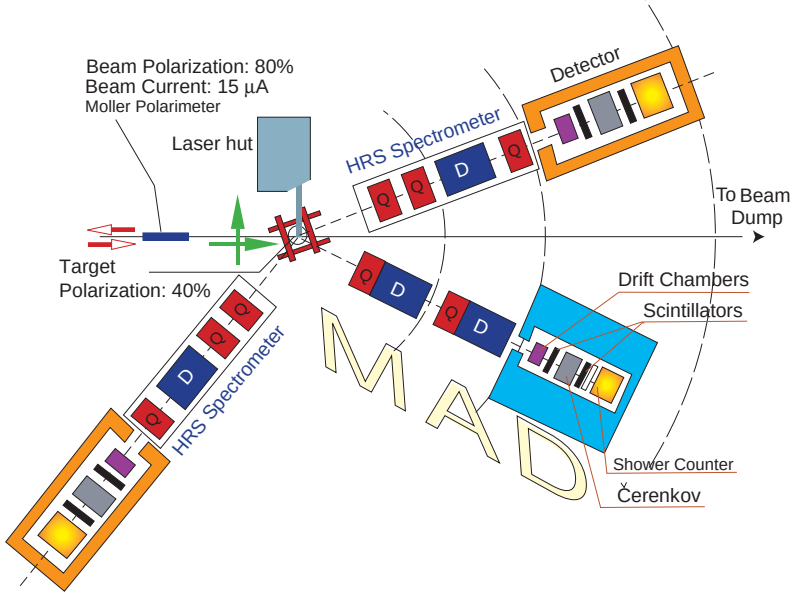

Figure 16: *Lay-out of Hall A showing the configuration including the MAD spectrometer and the polarized* ^{3}*He target.*

are also intended, as well as measurements of the g_2^n spin structure function and its moments. The latter measurements will provide a clean measure of a higher twist effect (twist 3), which is related to the quark-gluon interaction.

A further discussion of the experiments listed is given in Ref. [13]. Three instrumentation upgrades are proposed to allow an optimal study of the intended experiments: a large acceptance spectrometer, an electro-magnetic calorimeter and a ^{3}H target. The proposed instrumentation is presented in more detail in Ref. [14].

2.2 The large-acceptance spectrometer

The spectrometer would provide a tool for high-x studies of the properties of nucleons with an 11 GeV beam, where a large acceptance in both solid angle and momentum coupled to a moderate momentum resolution are needed. The proposed MAD (Medium Acceptance Detector) device is a magnetic spectrometer built from two combined-function (quadrupole and dipole) superconducting magnets that can simultaneously produce a 1.5 T dipole field and a 4.5 T/m quadrupole field inside a warm bore of 120 cm. The quadrupole components provide the fo-

cusing necessary to achieve the desired solid angle while the dipole components provide the dispersion needed for momentum resolution. A magnetic design using TOSCA3D has been performed to establish the basic magnetic requirements and to provide 3D field maps for optics analysis. A two-sector $\cos(\phi)/\cos(2\phi)$ design with a low nominal current density has been selected and analyzed. Extra versatility can be achieved by varying the drift distance to the first magnet. Larger drift distances allow smaller scattering angles (down to 12°) at the cost of reduced acceptance. Optical properties and their impact on the performance have been studied, resulting in a momentum acceptance (resolution) of ± 15 (0.2)% and an angular acceptance (resolution) of 30 msr (2 mrad). The maximum central momentum is 6 GeV/c at a total bend angle of 20°, but can in principle be increased by decreasing the bend angle.

The basic detector package for the MAD spectrometer will serve for most electron scattering experiments. The detectors have been designed to cover the full momentum and angular acceptance. The design includes an optional hadron configuration with a flexible particle identification system in the trigger and a very powerful PID in the off-line analysis. The main components of the basic detector package are: high resolution drift chambers, a hydrogen gas Čerenkov counter, trigger scintillator counters and a lead glass hadron rejector. The main components of the hadron configuration are: a variable pressure gas Čerenkov counter, two diffuse reflective aerogel counters and a Ring Imaging Čerenkov counter. A conceptual design for the MAD support structure has been completed. The device can be withdrawn up the truck ramp to allow operation with the existing HRS pair (see Fig. 16).

2.3 High Performance Electromagnetic Calorimetry

A highly segmented total absorption calorimeter is proposed for use in conjunction with the magnetic spectrometers in high-luminosity Compton experiments (real and virtual) at 11 GeV. The calorimeter must combine high spatial resolution, good energy resolution, fast time response, and be very radiation hard. A calorimeter of 1000 PbF_2 crystals, each $2.5 \times 2.5 \times 15$ cm^3 is proposed. Each crystal will be coupled to a mesh PMT for optimum time resolution. The PMT signals will be digitized by a 1 GHz fast sampling ADC system, for off-line suppression of pile-up. PbF_2 is an attractive Čerenkov medium for electromagnetic calorimetry, but additional tests are required for the selection of calorimeter material.

The calorimetry requirements are most stringent for Deeply Virtual Compton Scattering (DVCS) in which an energetic photon must be detected in the direction of the $\vec{q}$-vector (angles as small as 10°) and with a luminosity of at least $10^{37}/\text{cm}^2/\text{s}$. It is important to resolve the exclusive DVCS process from competing inelastic processes. For different calorimetry materials, Fig. 17 illustrates the kinematic limit for separation at the 1-σ level of the exclusive channel by $p(e, e'\gamma)X$ double coincidences alone. Beyond the limits illustrated in the figure,

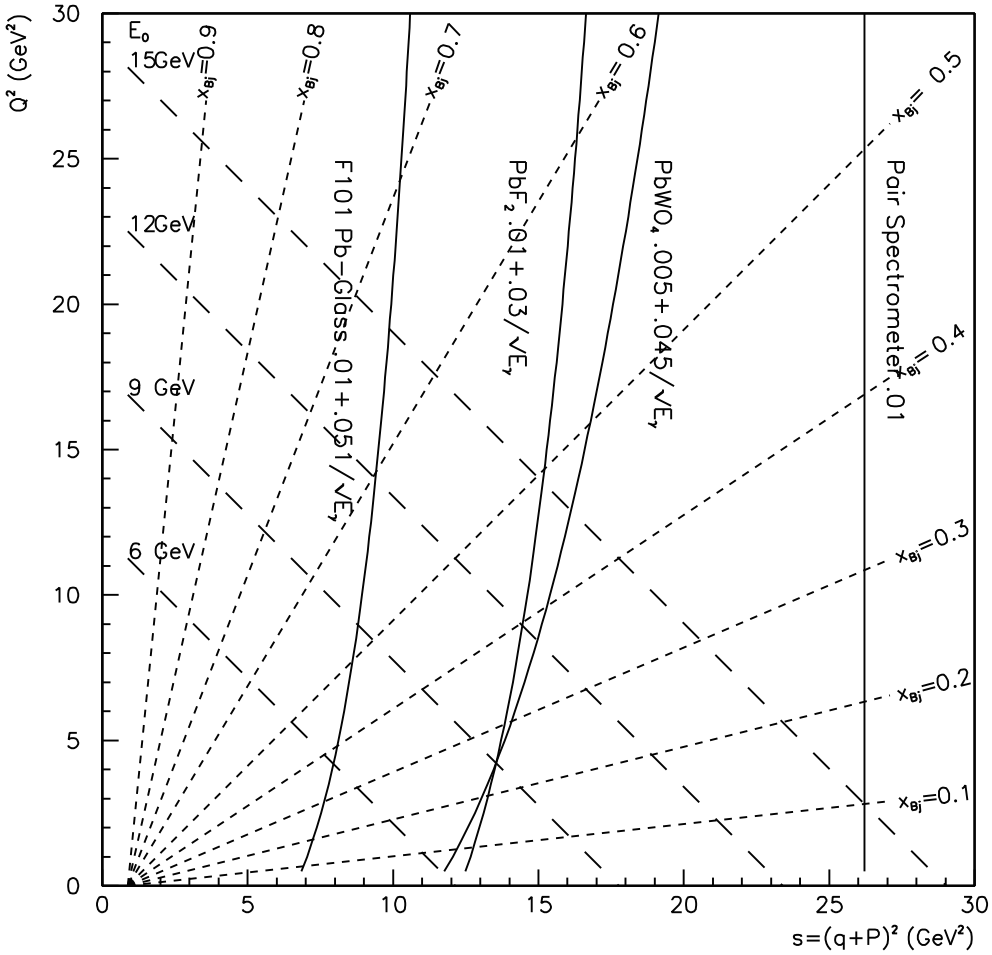

Figure 17: *Photon resolution on a plot Q^2 vs. s. Contours of constant $x_{\rm Bj}$ and constant incident energy E_0 are indicated separately.*

the exclusive $ep \to ep\gamma$ channel can be resolved by detecting the recoil proton in triple coincidence. In the DVCS limit, the angular resolution required on the detection of the proton is approximately a factor of 10 less stringent then the requirements for the photon. A high performance calorimeter can greatly enhance the capabilities for real and virtual Compton scattering experiments at 11 GeV, and other experiments will no doubt also benefit from such a detector.

2.4 A ^{3}H Target

The major considerations in the design of the tritium target are: minimize the amount of tritium, minimize the uncertainty in density, match the spectrometer acceptance, and maximize the luminosity. For safety considerations, the maximum

amount of tritium should not exceed 30 kCi. Because of the ability to do coincidence experiments, the better match to the spectrometer solid angle, less stringent cooling requirements, and the more stable density as a function of current, a gas target is preferred, with a storage bed to remove the tritium from the target to a mechanically strong container for work on the target or for safety reasons. The major improvement required for the hall will be a tritium exhaust stack in order to vent the tritium out of the hall with sufficient height and speed to keep the exposure at ground level to an acceptable level.

3 Summaries of Experimental Activities

3.1 E89-019/E94-012/E99-008

Deuteron Photodisintegration and π^0 Photoproduction from the Proton

R. Gilman, R. Holt, and Z.-E. Meziani, Spokespersons,
and
the Hall A Collaboration.

These three experiments shared beamtime during the period from August through early November, 1999. E89-019 measured recoil proton polarization in deuteron photodisintegration at $\theta_{\rm cm} = 90°$ for photon energies form 0.5 to 2.5 GeV. With these measurements requiring only the hadron arm, E99-008 measured angular distributions of the photodisintegration cross section parasitically, using the electron arm set for positive polarity. E94-012 measured the reaction $\gamma p \to p\pi^0$, using both spectrometers so that the *ep* scattering could be identified.

The analysis of E89-019 is complete. Results have been presented at several conferences, and a paper (K. Wijesooriya *et al.*) submitted to Physical Review Letters on Sep. 15, 2000. Polarimeter calibrations during the experiments also generated a number of measurements of the proton form factors, for which the analysis is complete.

Analysis for the cross-section measurements of E99-008 forms part of the Ph.D. thesis of E. Schulte (U. of Illinois), who is also analyzing higher energy photodisintegration cross sections from Hall C E96-003. At three beam energies, 1.67, 1.95, and 2.5 GeV, eight point angular distributions for the cross section were measured, with $\theta_{\rm cm} = 30°$ to $143°$. With the Hall C results nearly final, analysis of E99-008 is now underway.

E_e	$45°_{\rm cm}$	$60°_{\rm cm}$	$75°_{\rm cm}$	$90°_{\rm cm}$	$105°_{\rm cm}$	$120°_{\rm cm}$
0.86	√	√	√	√	√	√
1.15	-	-	-	√	-	√
1.27	-	-	√	√	√	√
1.67	√	√	√	√	√	√
1.95	√	√	√	√	√	√
2.50	√	√	√	√	√	√
3.12	-	-	√	√	√	√
4.11	-	-	√	√	√	√
4.80	-	-	-	-	√	-

Table 9: *Kinematic coverage of E94-012 measurements.*

E94-012 was intended as a short survey of π^0 photoproduction. We attempted to measure angular distributions for the recoil proton polarizations, with one to

two days of beam time at each energy. A summary of the data points taken is given in Table 9. Note that the angles given are the proton angles, not the π^0 angles. With one exception, data was taken for every angle and energy planned. With polarized beam at all energies except 1.15 GeV, polarization transfer coefficients can be determined as well as induced polarizations.

With the analysis of E89-019 complete, Krishni Wijesooriya and Xiaodong Jiang have now started on the analysis of E94-012. Some preliminary results were presented at the Williamsburg Division of Nuclear Physics meeting during October, 2000.

3.2 E89-028

Polarization Transfer Measurements in the $D(e,e'p)n$ Reaction

P. E. Ulmer, J. M. Finn and M. K. Jones , Spokespersons,
and
K. Baker, E. Chudakov, A. Cochran, J. Calarco, S. Dumalski, R. Ent,
S. Frullani, F. Garibaldi, S. Gilad, R. Gilman, C. Glashausser, V. Gorbenko,
J. Hovebo, B. Hu, X. Jiang, T. Keppel, A. Klein, S. Kuhn, G. Kumbartski,
P. Markowitz, D. Meekins, J. Mitchell, Z. Papandreou, C. Perdrisat, V. Punjabi,
R. Roche, D. Rowntree, L. Todor, G. Urciuoli, K. Wijesooriya, R. Woo.

The goal of this experiment is to provide a test of the validity of deuteron models by providing data on the recoil polarization observables in d$(\vec{e},e'\vec{p})$n. In addition to enhancing our understanding of the deuteron structure and reaction mechanisms in $(e,e'p)$, the information gained here will be critical in interpreting the $G^n{}_E$ experiment of Madey *et al.* The Madey experiment employs an analogous reaction, d$(\vec{e},e'\vec{n}\,)$p, to extract the ratio of the neutron form factors $G^n{}_E/G^n{}_M$, assuming that the deuteron provides a source of essentially free neutrons. Various calculations suggest that polarization transfer at quasifree kinematics is expected to be free from the effects which have frustrated extraction of form factors in Rosenbluth L/T separations, most notably final state interactions (FSI). However, the $G^n{}_E$ measurement cannot test the quasifree assumption. Experiment E89-028 can test this assumption by comparing measurements on hydrogen and deuterium targets.

E89-028 measured the recoil polarization observables of the ^{1}H$(\vec{e},e'\vec{p}\,)$ reaction and the ^{2}H$(\vec{e},e'\vec{p}\,)$ reaction in quasifree kinematics (*i.e.* centered at zero recoil momentum) at the three Q^2 points of the Madey experiment: 0.43, 1.0 and 1.61 (GeV/c)^2. In Fig. 18, the $G^p{}_E/G^p{}_M$ ratio measured for ^{1}H$(\vec{e},e'\vec{p}\,)$ in this experiment is plotted and compared to previous measurement of E93-027 [15]. The agreement with the previous experiment is excellent.

In Fig. 19, preliminary results for the double ratio of the ratio of transverse, P_T, to longitudinal, P_L, polarization for ^{2}H$(\vec{e},e'\vec{p}\,)$ to the ratio for ^{1}H$(\vec{e},e'\vec{p}\,)$ are plotted. Only statistical error bars are shown. The ^{1}H$(\vec{e},e'\vec{p}\,)$ and ^{2}H$(\vec{e},e'\vec{p}\,)$ data were taken at exactly the same spectrometer settings, so that systematic errors would be minimized when measuring the ratio of polarization variables. Previous measurements [16] of the ^{2}H$(\vec{e},e'\vec{p}\,)$ reaction, from an experiment at Bates, are plotted in Fig. 19. Where the two data sets overlap at low Q^2, they agree. The new JLab data exhibit a significant reduction of the statistical error bar.

Since the Madey experiment will need to sample a fairly large range of recoil momenta (in order to achieve the required statistical precision), it is also important to test the quasifree assumption away from zero recoil momentum. Measurements were made of the three polarization components of ^{2}H$(\vec{e},e'\vec{p}\,)$ at $Q^2 = 1$ (GeV/c)^2 and centered at recoil momentum of 160 MeV/c, which spans

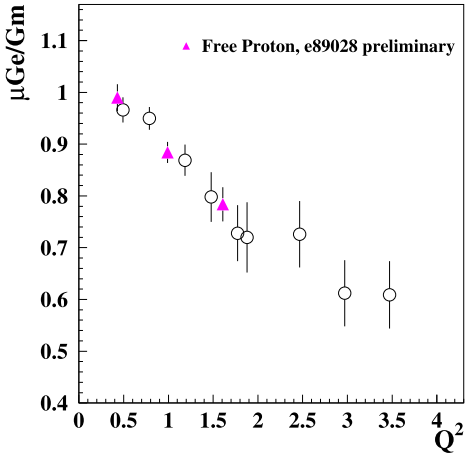

Figure 18: *Comparison between G_{Ep}/G_{Mp} for the $^1H(\vec{e}, e'\vec{p})$ reaction measured in E89-028 and in E93-027 (open circles) [15].*

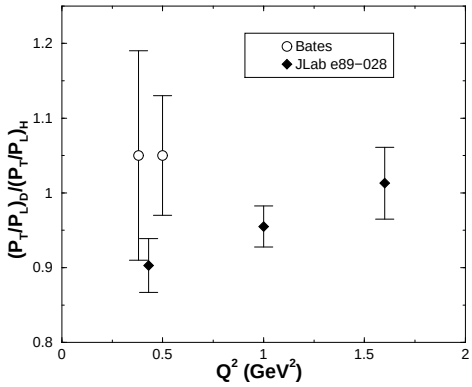

Figure 19: *Preliminary results for the double ratio, $(P_T/P_L)_D/(P_T/P_L)_H$, of the ratio of transverse to longitudinal polarization for $^2H(\vec{e}, e'\vec{p})$ to the ratio for $^1H(\vec{e}, e'\vec{p})$. The open circles are measurements from Ref. [16]*

the range of the Madey experiment. The longitudinal and transverse components of the polarization were measured to a precision of 5%. At this recoil momentum, the measurement of the normal polarization, which is zero in the absence of FSI, will provide another constraint for this important aspect of the theory. At this point, we need to make comparisons to theoretical calculations before any conclusions can be drawn and a paper submitted.

3.3 E89-044

Selected Studies of the ^{3}He and ^{4}He Nuclei through Electrodisintegration at High Momentum Transfer

D. W. Higinbotham for the E89-044 Collaboration [1]

Coincidence experiments have proven to be very useful tools in studying specific aspects of the nucleus. In particular the (e,e'p) reaction has been used not only to study the single-nucleon structure of nuclei but also to study the behavior of nucleons embedded in the nuclear medium. The high energy, high duty cycle beam at Jefferson Lab will allow us to fully develop such studies. This will be accomplished by extending the domain of momentum transfers towards higher values where short-range effects and possibly the internal structure of the nucleons are manifested, by exploring nuclear structure in its extreme conditions, by investigating the high momentum part of the wave functions, and by increasing the specificity of the probe by separating the response functions associated with different polarization states of the virtual photon.

The E89-044 collaboration plans to exploit these new possibilities by undertaking a series of (e,e'p) measurements on the Helium isotopes. Next to the deuteron, the A=3 and A=4 nuclei are the simplest systems in which all the basic ingredients of a complex nucleus exist. Sophisticated methods to solve the Schrödinger equation almost exactly have been applied to the A=3 nuclei and have been extended to ^{4}He. Microscopic calculations of FSI and MEC contributions have been developed and applied to reactions on few-nucleon systems. The data provided by the E89-044 experiment will test the validity of these models in the high Q^2 and high missing momentum regime.

The collaboration completed the ^{3}He(e,e'p) portion of this study in March, 2000, after receiving nearly three months of beam time. In perpendicular kinematics, with a constant momentum transfer of 1.5 GeV/c and a constant energy transfer of 0.837 GeV, cross sections were measured at missing momentum 0, 150, 300, 425, 550, 750, and 1000 MeV/c. The R_{L+TT}, R_T, and R_{LT} response functions will be extracted for missing momenta of 0, 150, 300, 425, and 550 MeV/c. In parallel kinematics, where the proton is emitted in the direction of the momentum transfer vector, the Q^2 dependence from 0.8 to 4.1 [GeV/c]^2 will be determined by performing longitudinal/transverse separations. These measurements were performed for -300, 0, 300 MeV/c missing momentum and for momentum transfers 1.0, 1.9 and 3.0 GeV/c. In addition, the experiment measured cross sections in the continuum region to study correlated nucleon pairs.

An overview of the measured kinematics is shown in Table 10. The missing energy and missing momenta spectra from one of the high missing momentum kinematics, Kin 10, is shown in Figure 3.3. The scaler information from these

[1] http://hallaweb.jlab.org/physics/experiments/E89-044/collaboration.ps

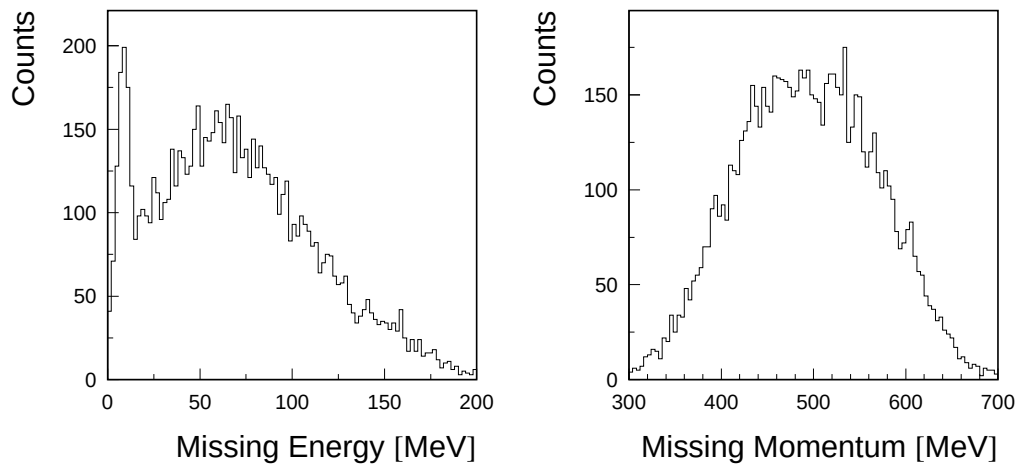

Figure 20: *Shown on the left is the missing energy spectrum for perpendicular kinematics 10. The two-body break-up peak can be seen around 5.5 MeV while the strength in the continuum region is seen at the higher missing energies. Shown on the right is the missing momentum spectrum for the same kinematics.*

measurements has been placed in a MySQL database located at http://marat-rvachev2.jlab.org/php. To normalize the measured ^{3}He cross sections, extensive single-arm elastic scattering data was taken. Between elastic scattering measurements, single arm events were recorded to monitor relative luminosity during the ^{3}He(e,e'p) measurements. Combining the known elastic cross sections with our luminosity monitoring data will provide an absolute normalization for the ^{3}He(e,e'p) cross sections.

The analysis of the data is being performed primarily by four groups, CalState, Grenoble, MIT, and Rutgers. Three graduate students, Fatiha Benmokhtar (Rutgers), Emilie Penel (Grenoble), Marat Rvachev (MIT), will receive their dissertation data from this experiment. Also, several undergraduates at CalState have been working with the elastic scattering data to get their first experience analyzing nuclear physics data. Further details and up to data information on the analysis can be found at http://hallaweb.jlab.org/physics/experiments/E89-044.

Perpendicular Kinematics	$\vec{q}$ [GeV/c]	E_0 [GeV]	ω [GeV]	ϵ	P_m [GeV/c]
Kin01	1.50	4.80	0.837	0.943	0.00
Kin02	1.50	4.80	0.837	0.934	0.00
Kin03	1.50	1.25	0.837	0.108	0.00
Kin04	1.50	4.80	0.837	0.943	0.150
Kin05	1.50	4.80	0.837	0.943	0.150
Kin06	1.50	1.25	0.837	0.108	0.150
Kin07	1.50	4.80	0.837	0.943	0.300
Kin08	1.50	4.80	0.837	0.943	0.300
Kin09	1.50	1.25	0.837	0.108	0.300
Kin10	1.50	4.80	0.837	0.943	0.425
Kin11	1.50	4.80	0.837	0.943	0.425
Kin12	1.50	1.25	0.837	0.108	0.425
Kin13	1.50	4.80	0.837	0.943	0.550
Kin14	1.50	4.80	0.837	0.943	0.550
Kin15	1.50	1.25	0.837	0.108	0.550
Kin28	1.50	4.80	0.837	0.943	0.750
Kin29	1.50	4.80	0.837	0.943	1.00
Kin31	1.50	1.25	0.880	0.069	0.401
Kin32	1.50	1.25	0.880	0.069	0.509
Kin33	1.50	1.95	0.837	0.615	0.000
Kin34	1.50	1.95	0.837	0.615	0.150
Kin35	1.50	1.95	0.837	0.615	0.150
Parallel Kinematics	$\vec{q}$ [GeV/c]	E_0 [GeV]	ω [GeV]	ϵ	P_m [GeV/c]
Kin16	1.00	4.04	0.438	0.966	0.00
Kin17	1.00	0.845	0.438	0.221	0.00
Kin18	1.94	4.80	1.22	0.898	0.00
Kin19	1.94	1.95	1.22	0.314	0.00
Kin20	3.00	4.80	2.21	0.718	0.00
Kin21	3.00	2.90	2.21	0.180	0.00
Kin22	1.00	2.90	0.700	0.925	-0.300
Kin23	1.00	1.25	0.700	0.527	-0.300
Kin24	1.94	4.80	1.52	0.891	-0.300
Kin25	1.94	1.95	1.52	0.204	-0.300
Kin26	1.00	4.05	0.262	0.968	+0.300
Kin27	1.00	0.845	0.262	0.342	+0.300
Kin36	1.00	1.95	0.439	0.847	0.000

Table 10: *The perpendicular and parallel kinematics measured during the recently completed E89-044* ^{3}*He(e,e'p) experiment.*

3.4 E91-010

The Hall A Proton Parity Experiment (HAPPEX)

J.M. Finn and P.A. Souder, Spokespersons,
and
the HAPPEX and Hall A Collaborations.

HAPPEX has measured the parity-violating electroweak asymmetry in the elastic scattering of polarized electrons from the proton. This experiment took place in Hall A at the Thomas Jefferson National Accelerator Facility. An approximately 35μA beam of 67-76% polarized electrons with an energy of 3.3 GeV scattered from a 15 cm liquid hydrogen target. Elastic events were detected by integrating the signal in total-absorption counters located at the focal plane of a pair of high-resolution magnetic spectrometers. [17] This measurement is the first fixed-target parity violation experiment that used either a "strained" GaAs photocathode to produce highly polarized electrons or a Compton polarimeter to continuously monitor the electron beam polarization.

Strange form factors can be isolated from up and down quark form factors by measuring the parity-violating asymmetry $A = (\sigma_R - \sigma_L)/(\sigma_R + \sigma_L)$ in the elastic scattering of polarized electrons from protons. The experiments are challenging since $A \approx A_0\tau \approx 10$ parts per million (ppm) for typical kinematics. Here $A_0 = (G_F M_p^2)/(\sqrt{2}\pi\alpha) = 316.7$ ppm, where G_F is the Fermi constant for muon decay and M_p is the proton mass. Also $\tau = Q^2/4M_p^2$ where Q^2 is the square of the four-momentum transfer. Nevertheless, several experiments have recently published significantly non-zero values for A [17–19].

Measurements of elastic electromagnetic and electroweak nucleon scattering provide three sets of vector form factors. From this information, the form factors for each of the light flavor quarks may be determined [20]: $G^u_{E,M}$, $G^d_{E,M}$, and $G^s_{E,M}$. A convenient alternate set, which is directly accessible in experimental measurements, is the electromagnetic form factors $G^{p\gamma}_{E,M}$, $G^{n\gamma}_{E,M}$, plus $G^0_{E,M}$. Here $G^0 = (G^u + G^d + G^s)/3, G^{p\gamma} = \frac{2}{3}G^u - \frac{1}{3}G^d - \frac{1}{3}G^s$,and $G^{n\gamma} = \frac{2}{3}G^d - \frac{1}{3}G^u - \frac{1}{3}G^s$,where the last expression assumes charge symmetry.G^0 cannot be accessed in electromagnetic scattering and thus represents new information on nucleon dynamics that can be accessed only via measurements of the weak neutral current amplitude.

The theoretical asymmetry in the Standard Model has a convenient form in terms of G^0:

$$A_{th} = -A_0\tau\rho'(2 - 4\hat{\kappa}\prime_{eq}\sin^2\theta_W - \frac{\varepsilon\eta_p}{\varepsilon\eta_p^2 + \tau\mu_p^2}\frac{G^0_E + \beta G^0_M}{(G^{\gamma p}_M/\mu_p)}) - A_A$$

where $\mu_p(\mu_n) \approx 2.79(-1.91)$ is the proton(neutron) magnetic moment in nuclear magnetons,$\eta_p = \eta_p(Q^2) = G^{p\gamma}_E(Q^2)/(G^{p\gamma}_M(Q^2)/\mu_p), \varepsilon = (1 + 2(1+\tau)\tan^2\theta/2)^{-1}$ is

thelongitudinal photon polarization, and $\beta = \tau\mu_p/(\varepsilon\eta_p)$. The scattering angle of the electron in the laboratory is θ. The contribution from the proton axial form factor, $A_A = (0.56 \pm 0.23)$ ppm, is calculated to be small for our kinematics [21, 22]. Recent data from the SAMPLE collaboration [23] is not inconsistent with Refs. [21,22] but has larger errors. The parameters $\rho\prime_{eq} = 0.9879$ and $\hat{\kappa}\prime_{eq} = 1.0029$ include the effect of electroweak radiative corrections [24],and $\sin^2\theta_W = 0.2314$.

If, in addition to $G^0_{E,M}$, the proton and neutron electromagnetic form factors $G^{p\gamma}_{E,M}$ and $G^{n\gamma}_{E,M}$ are known, the strange form factors may be determined from

$$G^s_{E,M} = G^0_{E,M} - G^{p\gamma}_{E,M} - G^{n\gamma}_{E,M}.$$

It is convenient to normalize the form factors to $G^{p\gamma}_M/\mu_p$since the normalized form factors depend less on experimental uncertainties and tend to vary less with τ. The quantities extracted are $G^s_E/(G^{p\gamma}_M/\mu_p) \to \tau\rho_s$ and $G^s_M/(G^{p\gamma}_M/\mu_p) \to \mu_s$ for the limit $\tau \to 0$. Models suggest that the radius parameter ρ_s could be of the order of ± 2 and the strangeness contribution to the magnetic moment μ_s could be of the order of -0.3. If the strange form factors are indeed of this scale, our experiment along with other experiments in progress should be able to establish their presence.

It is important that the signal be purely elastic, since background processes may have large asymmetries. For example, the production of the prominent $\Delta-$resonance has 3 times the asymmetry of elastic scattering. [20] To measure the rejection of unwanted events by our system, we measured the response of the detector, both in counting and integrating mode, as a function of the mismatch between the spectrometer setting and the momentum of elastic events. Based on these data, we determined that only 0.2% of our signal arises from inelastic background processes. Quasi-elastic scattering from the Al target windows contributed 1.5% to the measured signal.

A new feature of the experiment is that the beam polarization $P_e \approx 70\%$. This was achieved by using photoemission by circularly polarized laser light impinging on a "strained" GaAs crystal. The Compton device continuously monitored the polarization of the beam on target and ruled out possible significant variations in polarizations between the daily Møller measurements. Both devices have an overall systematic error $\Delta P_e/P_e \sim 3.2\%$.

To study possible systematic errors in our small asymmetry, we inserted a half-wave ($\lambda/2$) plate in the laser beam at the source to reverse the sign of the helicity. Data were obtained in sets of 24-48 hour duration, and the state of the $\lambda/2$ plate was reversed for each set. The resulting asymmetries are shown in Fig. 21a. The asymmetries reverse as expected but otherwise behave statistically. The strained GaAs crystal, in contrast to the bulk GaAs used for our previous result, has a large analyzing power for linearly polarized light.

The analyzing power tends to promote helicity-correlated differences in beam parameters such as position, energy, and intensity. The intensity asymmetry was

nulled with a feedback system. In addition, the intensity asymmetry in the beam in another hall also had to be nulled.

The position and energy differences were measured with precision microwave monitors. One example of monitor data is shown in Fig. 21b. The effect of these beam differences on the asymmetry was measured by calibrating the apparatus with beam correction coils and an energy vernier. The resultant correction, shown in Fig. 21c, proved to have an average of 0.02 ± 0.02 ppm.

The experimental asymmetry, corrected for the measured beam polarization, is $A_{exp} = -15.1$ ppm at $Q^2 = 0.477$ (GeV/c)^2 for the 1999 data.We also include the previously reported 1998 data, [17] which gives $A_{exp} = -14.7$ ppm when extrapolated to the same Q^2 value but with approximately twice the statistical and systematic errors.

In addition, three small corrections based on subsequent data analysis were made to the 1998 data: i. the background correction was included; ii. the measured beam polarization was reduced by 1.5%; and iii. the Q^2 value was determined to be 0.474 (GeV/c)^2. instead of 0.479 (GeV/c)^2. An increase of 1% in Q^2 is expected to increase the magnitude of the asymmetry by 1.5%.

Systematic errors in the beam polarimetry and in the measurement of the spectrometer angle were the most significant sources.The combined result is $A_{exp} = -15.05 \pm 0.98(stat) \pm 0.56(syst)$ ppm at the average kinematics $Q^2 = 0.477$ (GeV/c)^2 and $\theta = 12.3°$. This is the average asymmetry over the finite solid angle of the spectrometers; we estimate the value at the nominal kinematics is smaller by 0.7%. We obtain $(G_E^0 + \beta G_M^0)/(G_M^{p\gamma}/\mu_p) = 1.527 \pm 0.048 \pm 0.027 \pm 0.011$, where the first error is statistical, the second systematic, and the last error is due to the uncertainty from A_A; $\beta = 0.392$ in our kinematics. The sensitivity to η_p is negligible. For our kinematics, $(G_M^{p\gamma}/\mu_p) \sim 0.36$.

We analyse the contribution due to strange form factors in a paper that we have recently submitted to Physics Letters.

We wish to thank the entire staff at JLab for their tireless work in developing this new facility, and particularly C. K. Sinclair and M. Poelker for their timely work on the polarized source. This work was supported by DOE contract DE-AC05-84ER40150 under which the Southeastern Universities Research Association (SURA) operates the Thomas Jefferson National Accelerator Facility, the Department of Energy, the National Science Foundation, the Korean Science and Engineering Foundation (Korea), the INFN (Italy), the Natural Sciences and Engineering Research Council of Canada, the Commissariat à l'Énergie Atomique (France), and the Centre National de Research Scientifique (France).

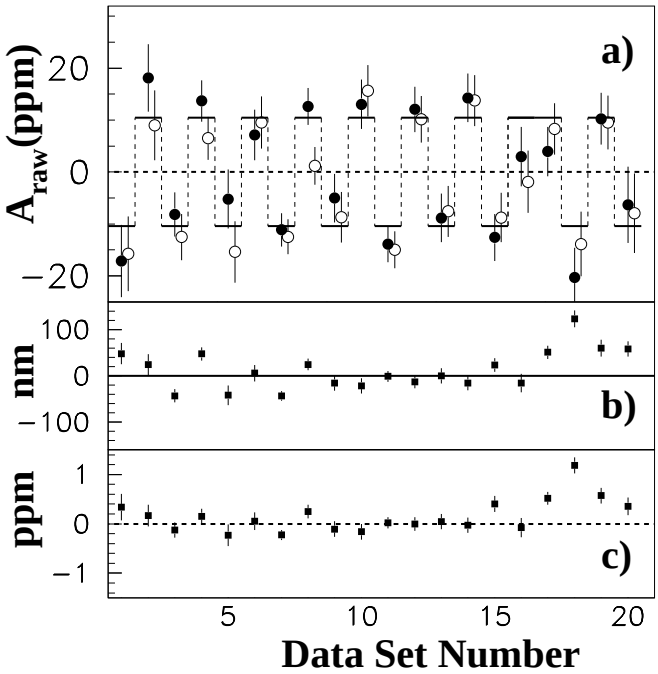

Figure 21: *(a) Raw asymmetry versus data set. Solid(open) circles are from the left(right) spectrometer. The step pattern is due to the insertion of the half-wave plate. The* $\chi^2 = 33.7$ *for 39 degrees of freedom. b) Helicity-correlated horizontal position difference measured near the target. c) Correction to left spectrometer data due to all of the beam parameter differences.*

3.5 E91-011

Investigation of the $N \to \Delta$ Transition via Polarization Observables in Hall A

S. Frullani, J.J. Kelly, and A.J. Sarty, Spokespersons,
and
the Hall A Collaboration.

Recoil polarization observables can provide new insight into properties of nucleon resonances and the reaction mechanisms for electroproduction of mesons by providing access to interference between small amplitudes and dominant amplitudes. The dominant amplitude for pion electroproduction at the Δ resonance is the M_{1+} multipole, but there is much current interest in the smaller S_{1+} amplitude that arises from configuration mixing within the quark core [25], often described as quadrupole deformation, or from meson and gluon exchange currents between quarks [26], or coupling to the pion cloud outside the quark core [27,28]. Observables which depend upon real parts of interference products are sensitive to these quadrupole amplitudes, but reliable interpretation of such data requires understanding background contributions from nonresonant production mechanisms and from underlying nondominant resonances. Sensitivity to background amplitudes is provided by observables which depend upon the imaginary parts of similar interference products. Experiment E91-011 was designed to measure both types of observables for the $p(\vec{e}, e'\vec{p})\pi^0$ reaction using the focal-plane polarimeter.

The experiment ran between May 19 and July 31, 2000, and received an average current of 45 μA for 36.5 days, corresponding to about 64% of scheduled calendar time. The beam polarization for several cathode locations varied between 67 and 79% and was monitored almost continuously by the Compton polarimeter. Polarized beam was delivered to Hall A during the June 8 to July 1 period using two lasers and achieved a record current of 110 μA with high polarization, although the lifetime was relatively short.

The production kinematics are summarized in Table 11. The nominal beam energy, $E_0 = 4.535$ GeV, electron scattering angle, $\theta_e = 14.09°$, and scattered electron momentum, $k_f = 3.066$ GeV/c, were constant for the production data. The proton momenta and angles were chosen to give central values of $W = 1.232$ GeV and $Q^2 = 1.0$ (GeV/c)^2 while optimally covering the center-of-mass angular distribution. The table lists nominal center-of-mass angles θ_{cm} where positive (negative) angles refer to nucleon momenta forward (backward) with respect to the virtual photon momentum $\vec{q}$. The total charge collected for each setting is given in coulombs. For each setting, a portion of the data was collected with 6 msr collimators in each spectrometer, but for most settings the bulk of the data was acquired without collimators. Extensive measurements for optics, pointing, luminosity, and dead time were made also.

The high singles rates on the forward side of $\vec{q}$ and relatively large π^+ contamination necessitate careful particle identification and background rejection.

Table 11: *Kinematics summary for E91-011.*

θ_{cm} deg.	θ_{lab} deg.	p_{lab} GeV/c	charge C
-155	49.72	0.742	11.5
-135	53.64	0.819	20.2
-90	54.79	1.066	13.7
-50	50.18	1.270	10.5
-25	46.33	1.350	4.6
0	42.30	1.378	16.7
25	38.12	1.350	6.2
50	34.29	1.270	13.0
90	29.81	1.066	12.0
135	30.81	0.819	11.1
155	34.71	0.742	11.1
180	42.28	0.703	3.8

Figure 22 illustrates the effectiveness of several selection criteria. A cut on the correlation between vertex position and coincidence time eliminates most of the accidental coincidences. A cut on mean pulse height in the scintillators versus β eliminates most of the pion contamination. An aerogel detector was used for most of the forward-angle running to reduce the trigger rate and dead time contributed by pions. An additional cut on missing energy versus missing mass also reduces background, particularly on the large-angle side of $\vec{q}$ where the elastic radiative tail is responsible for the strong peak at small missing mass; this peak is cut off on its lower side by acceptance. Very little background remains under the final missing-mass peak. Note that the missing-mass resolution is better on the large-angle than on the small-angle side of $\vec{q}$ where the sensitivity to angular resolution is greater.

Even though the hadron spectrometer is confined to a horizontal plane, Fig. 23 demonstrates that kinematic focusing of the reaction cone to a laboratory opening angle of about 13° provides considerable out-of-plane acceptance. The nearly complete coverage for $\theta_{cm} < 50°$ will permit extraction of response functions which require out-of-plane momenta. Therefore, we have developed an analysis procedure that exploits the various ϕ dependencies of cross section and polarization observables to extract most of the response functions that do not require Rosenbluth separation. This procedure was tested by Monte Carlo simulation before the experiment and will be applied to the data after the calibration analysis. The data analysis is proceeding smoothly and we expect to have preliminary data for polarized and unpolarized response functions by spring of 2001.

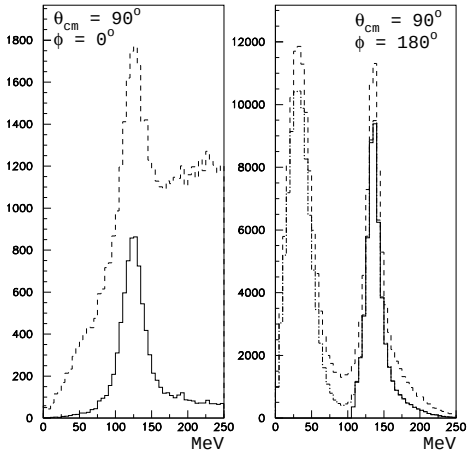

Figure 22: *The effectiveness of event selection criteria is illustrated for* $\theta_{cm} = \pm 90°$. *The dashed curves have only a loose cut on coincidence time; the dash-dotted curves have cuts applied to both coincidence time versus reaction-vertex and* β *versus pulse-height particle identification; and the solid curves add a cut to select pion production in* E_m *versus* p_m.

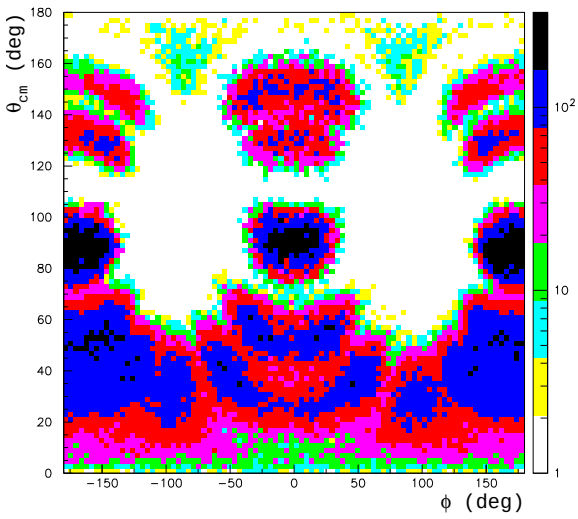

Figure 23: *Angular acceptance for* $1.207 \leq W \leq 1.257$ *GeV and* $0.9 \leq Q^2 \leq 1.1$ *(GeV/c)*^{2}. *Contours of normalized yield are shown for* (θ_{cm}, ϕ_{cm}), *combining the various spectrometer settings.*

3.6 E93-049

Polarization Transfer in the Reaction ^{4}He$(\vec{e}, e'\vec{p})\,^3$H in the Quasi-elastic Scattering Region

R. Ent and P.E. Ulmer, Spokespersons,
and
the E93-049 Collaboration.

Experiment E93-049 measured polarization observables in the ^{4}He$(\vec{e}, e'\vec{p})\,^3$H reaction at Q^2 of 0.5, 1.0, 1.6, and 2.6 (GeV/c)^2. Data taking was completed in May of 2000.

Polarization transfer in quasi-elastic nucleon knockout is sensitive to the properties of the nucleon in the nuclear medium including possible modification of the nucleon form factor and/or spinor. The experiment consisted in measuring the polarization transfer coefficients over the range of Q^2 from 0.5 to 2.6 (GeV/c)^2 and as a function of missing momentum in the range 0 to 250 MeV/c in order to determine the electric to magnetic form factor ratio for protons bound in the ^{4}He nucleus. ^{4}He was selected for study since its relative simplicity allows for realistic microscopic calculations and since its high density enhances any possible medium effects. Also, a variety of calculations indicate polarization observables for the ^{4}He$(\vec{e}, e'\vec{p})\,^3$H reaction have minimal influence from final-state interactions (FSI) and meson-exchange currents (MEC). It is precisely these effects (especially FSI) that have so far prevented a clean determination of nucleon medium modifications from unpolarized response functions in $(e, e'p)$ experiments.

A recent calculation by D.H. Lu *et al.* [29] shown in Fig. 24 suggests a measurable deviation from the free space ratio over the Q^2 range of this experiment. Note that the calculation is consistent with present constraints on possible medium modifications for both the electric form factor (from the Coulomb Sum Rule, with $Q^2 < 0.5$ (GeV/c)^2), and the magnetic form factor (from a y-scaling analysis) for $Q^2 < 2$ (GeV/c)^2. The calculation seems to predict too large an effect for the magnetic form factor at higher Q^2; however, it has been suggested that in order to interpolate smoothly between confined and deconfined phases, as the baryon density increases the bag constant might decrease. Such an effect would reduce the Q^2 dependence of the medium modification of the magnetic form factor, while still having a measurable effect in the ratio of G_E/G_M. Similar measurable effects have been calculated in the model of Frank *et al.* [30].

As the experiment was designed to detect differences between the in-medium polarizations compared to the free values, both ^{4}He and ^{1}H targets were employed (due to beam time constraints, at $Q^2 = 2.6$ (GeV/c)^2 only ^{4}He data was acquired). The statistical precision for the polarization double ratio is roughly 5%, 4%, 4% and 10% at Q^2 of 0.5, 1.0, 1.6, and 2.6 (GeV/c)^2 respectively (the dominant error at the high Q^2 point is from our interpolation on the existing Hall A G_E/G_M

data for the proton from Jones *et al.* [15]). Systematic errors are expected to be significantly less than the statistical errors.

A first-pass analysis was recently completed. We have begun acceptance-averaged, radiatively-folded, calculations for comparison to data. Although the individual polarizations (and especially the induced normal component) are more sensitive to systematics than the polarization ratio, we plan to extract the individual components as well, as they provide additional constraints on reaction models for ^{4}He. This experiment forms the Ph.D. thesis project of Sonja Dieterich from Rutgers University. Two postdocs, Bitao Hu from Hampton University and Steffen Strauch from Rutgers University, are working on the analysis. We expect to have final results in about one year.

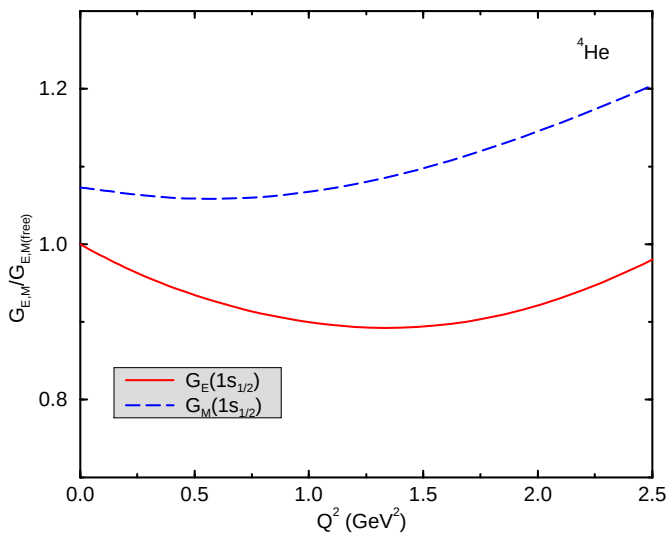

Figure 24: *Ratio of in-medium to free space electric and magnetic form factors of the proton in ^{4}He [29]. The free bag radius was taken to be 0.8 fm.*

3.7 E93-050

Virtual Compton Scattering

P.-Y. Bertin, P.A.M. Guichon, C.E. Hyde-Wright, co-spokespersons

In experiment 93-050 we measured the $H(e, e'p)\gamma$ reaction, using the Hall A cryotarget and the HRS^2 pair to detect the scattered electron and recoil proton in coincidence. To lowest order in α_{QED}, this reaction is a coherent superposition of radiation from the incident or scattered electron in elastic ep scattering (Bethe-Heitler–BH) and exclusive production of a photon on the proton, by absorption of a virtual photon (Virtual Compton Scattering–VCS). Experimentally, we separate the exclusive photon final state from π^0 electroproduction and other channels by reconstructing the missing mass of the unobserved particle(s). This experiment is the subject of the Ph.D. theses of N. Degrande (Gent), S. Jaminion (Clermont-Ferrand), C. Jutier (ODU - Clermont-Ferrand), G. Laveisière (Clermont-Ferrand), and L. Todor (ODU).

The kinematics of the VCS reaction are characterized by the invariant momentum transfer squared from the electron: $Q^2 = -q^2 = (k - k')^2$, the invariant mass of the photon-proton system: $s = W^2 = (q + P)^2$, and the polar and azimuthal angles $\theta_{\gamma\gamma}$ and $\phi_{\gamma\gamma}$ of the outgoing photon relative to the direction $\vec{q}$ of the momentum transfered from the electron.

The virtual compton amplitude includes a coherent sum of all possible intermediate states. In the low energy limit ($s \to M_p^2$, for arbitrary Q^2) the low energy theorems describe the VCS amplitude as a sum of the Born term (proton bremsstrahlung) plus a set of generalized polarizabilities.[31] The Q^2 variation of the generalized polarizabilities measures the spatial variation of the electric and magnetic polarization induced in the proton by external electric and magnetic fields.

In E93050, we took data below pion threshold ($M_p^2 < s < (M_p + m_\pi)^2$) at $Q^2 = 1.0$ and 1.9 GeV^2. In these measurements, a single electron arm setting spanned the entire region below threshold, and we moved the proton arm to span a large range in $\theta_{\gamma\gamma}$. At $Q^2 = 1$, we also measured a resonance excitation scan for nine central values of s from 1.3 GeV^2 to 3.6 GeV^2, with the coincidence angular kinematics centered on $\theta_{\gamma\gamma} = \pi$.

The VCS process in the nucleon resonance region is complementary to meson electroproduction. In particular, since this is a purely electromagnetic process, the VCS cross section should be a stringent test of resonance electroproduction amplitudes extracted from meson electroproduction.

In addition to physics data, we took extensive data in E93050 to calibrate the optics of the spectrometers at high momenta and with extended targets. The optics calibrations were done primarily with sieve slit data. To eliminate the depth of field problems from the extended target, we reconstructed the trajectories of elastically scattered electrons at the face of the colimator. An essential element

in these calibrations was the phase shift and attenuation in the instantaneous readout of the beam position monitors in the Hall A beam-line. We calibrated the beam energy by requiring agreement between the simulated and observed position of the missing mass peak. Typical values of the calibrated beam energy are 15 ± 3 MeV lower than the nominal 4045 MeV beam energy. The analysis is illustrated in Fig. 25 Details of these analysis can be found on the VCS web page.[32]

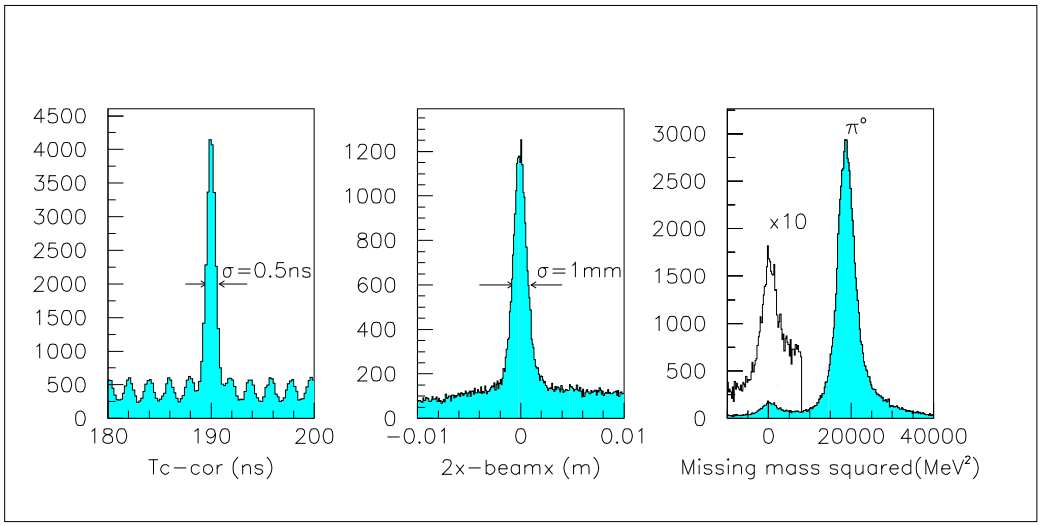

Figure 25: *VCS Analysis for setting $s = 2.5$ GeV^2 and $Q^2 = 1.0$ GeV^2. Left: Coincidence time of flight (ns) between the electron and proton arms, corrected for the path length variation in the two spectrometers. Middle: Two-arm-x – Beam-x (m). This is the the horizontal vertex coordinate reconstructed from the two spectrometers minus the instantaneous beam position. Right: $H(e, e'p)X$ missing mass squared, illustrating the VCS and π^0 peaks.*

Below pion threshold, we extract the differential cross section by comparing the integrated yield in a bin with a simulated cross section including the Bethe-Heitler and Born terms[33] and the radiative tail (second photon emission) of the complete VCS process.[34] Our preliminary cross sections at $Q^2 = 1.9$ GeV^2 are illustrated in Fig. 26. The gap in the angular distribution at $\theta_{\gamma\gamma}^{CM} \approx 100°$ corresponds to the two large BH peaks in the directions of the incident and scattered electrons. The broad peak at $\theta_{\gamma\gamma}^{CM} \approx -180°$ is dominated by the Born term (approximately a dipole radiation pattern from the recoil proton). At each angle $\theta_{\gamma\gamma}$ the effect of the polarizabilities will grow linearly with q'.

Fig. 27 shows the preliminary VCS cross sections in the nucleon resonance region, averaged over our ϕ-acceptance as a function of W in a bin of $\theta_{\gamma p}$ and Q^2. The Δ peak is shifted below 1230 MeV by the strong interference with the BH

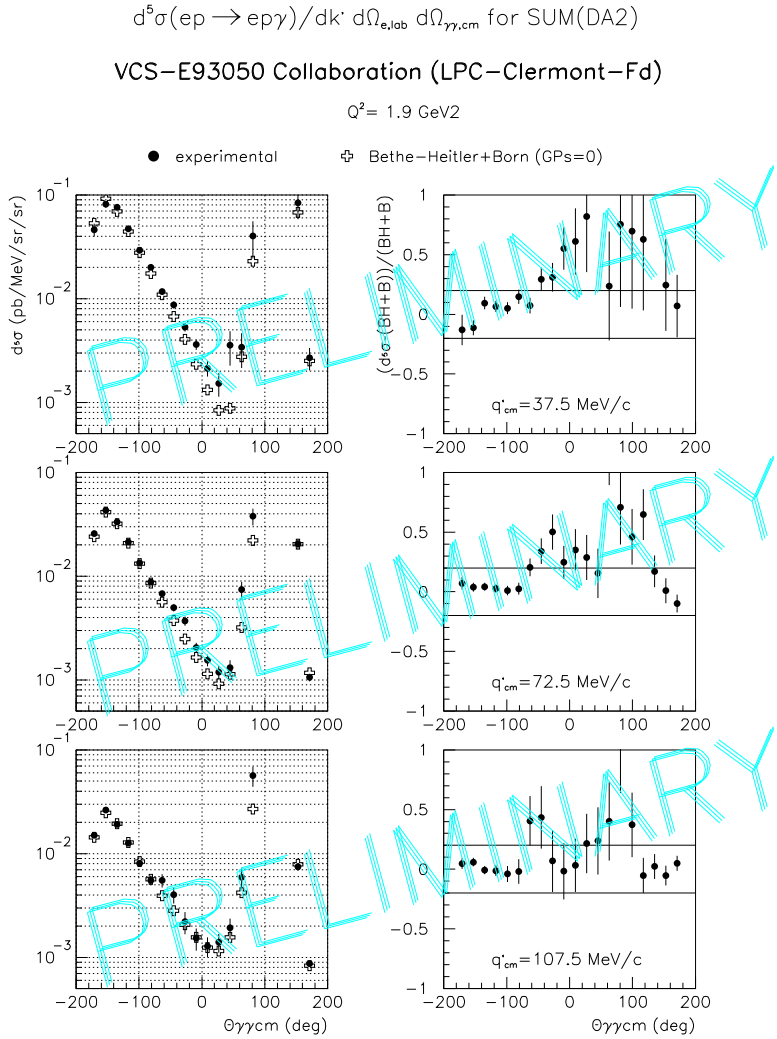

Figure 26: *VCS cross section below pion threshold. The kinematics are defined for* $Q^2 = 1.9\ GeV^2$ *and* $E_0 = 4.028\ GeV$. $q'_{CM} = (s - M^2)/(2\sqrt{s})$ *is the final photon energy in the photon-proton CM frame. Positive values of* $\theta^{CM}_{\gamma\gamma}$ *correspond to* $\phi_{\gamma\gamma} = 0$*; negative values of* $\theta^{CM}_{\gamma\gamma}$ *correspond to* $\phi_{\gamma\gamma} = \pi$*. The left hand plots show the differential cross section for* $q'_{CM} = 37.5$*, 72.5, and 107.5 MeV. The solid dots are the experimental cross section with statistical error bars. The open crosses are the cross sections from the low energy theorem (Bethe-Heitler + Born only). The right hand plots show the fractional deviation of the experimental results from the BH + Born theory. The systematic errors are estimated to be 15% in the angular domain* $[-180, -50] \cup [+150, +180]$ *and 25-30% in the angular domain* $[-50, +50]$.

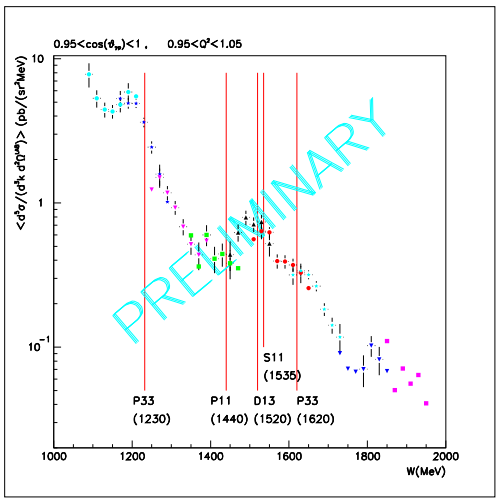

Figure 27: *VCS differential cross section in the nucleon resonance region, averaged over the experimental acceptance in* $\phi_{\gamma\gamma}$ *as a function of* W *in a bin* $0.95 < \cos\theta^{CM}_{\gamma p} \leq 1.0$ *and* $0.95 \leq Q^2 \leq 1.05$ GeV^2. $\theta^{CM}_{\gamma p}$ *is the angle between the* **q**-*vector and the recoil proton, in the photon-proton CM frame.*

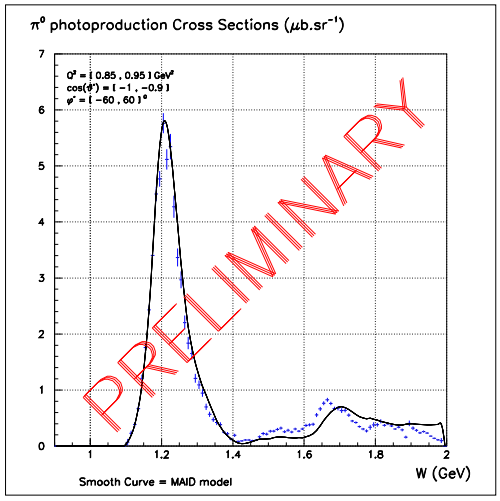

Figure 28: $H(\gamma^*, p)\pi^0$ *virtual photo-production cross section* $d\sigma/d\Omega^{CM}_{\gamma\pi}$ *averaged over the experimental acceptance within* $|\phi_{\gamma\gamma}| < 60°$, $-1.0 < \cos\theta' \leq -0.9$, *and* $0.85 \leq Q^2 \leq 0.95$ GeV^2, *as a function of* $W = \sqrt{s}$. θ' *is the angle between the virtual photon and the detected recoil proton, in the photon-proton CM frame.*

and Born amplitudes. The different symbols in the plot correspond to different spectrometer settings. The overlapping points are not necessarily expected to agree, since the ϕ-acceptance varies with W for each setting.

In Fig. 28 we present our cross sections for [virtual] photo-production of a π^0, averaged over our acceptance as a function of W in a bin in Q^2 and $\cos\theta^{CM}_{\gamma\pi}$. The solid line is the MAID[35] cross section model, averaged over the experimental acceptance. The integral of our result in the interval $1.15 < W < 1.35$ GeV agrees with the MAID model to within 7%. Phys. Rev. **C62**, 025501 (2000)

3.8 E94-004

In-plane Separations and High Momentum Structure in d$(e, e'p)$n

M.K. Jones and P.E. Ulmer, Spokespersons,
and
the Hall A Collaboration.

Experiment E94-004 involves separating the various response functions in the d$(e, e'p)$n reaction for a variety of quasi-elastic kinematics. The 3 calendar days of beam taken in October of 1999 (about 5% of the 29 days of approved beam time) were used to measure the unseparated cross section only. The cross section was measured at $Q^2 = 0.66$ (GeV/c)^2 for recoil momenta from 0 to 0.55 GeV/c. The electron kinematics were fixed and the recoil momentum range was spanned by varying the proton angle and momentum.

The deuteron, as the only bound two-nucleon system represents the simplest manifestation of the nuclear force. It therefore is a vital starting point from which to understand heavier nuclei including issues such as 3- or N-body forces and correlations. Understanding the deuteron is also necessary for the interpretation of various G_{En} measurements employing deuterium targets.

By examining high recoil momenta, this preliminary measurement gives access to the short distance character of the nucleon-nucleon (NN) interaction. Although high recoil momenta have been measured previously at Saclay and Mainz, the relatively low energies of these facilities compared to JLab required performing these measurements away from the quasi-elastic peak. Thus, contributions from meson-exchange currents and virtual nucleonic excitations make the extraction of information about the ground-state structure of the deuteron highly model dependent. In contrast, the higher beam energies of JLab allowed our experiment to be the first to sample high recoil momenta at quasifree kinematics, and thus we expect a cleaner interpretation in terms of deuteron structure.

We obtained statistics (per 20 MeV/c bin in recoil momentum) of 2% (4% for the highest recoil momenta). Systematic errors are expected to be roughly 5%. A first-pass analysis has been made and a preliminary spectrum will be available shortly. Pending the results of this analysis, we expect to submit an updated proposal to PAC19.

3.9 E94-010

Measurement of the Neutron (^{3}He) Spin Structure Function at Low Q^2; a connection between the BJ and DHG sum rules.

G.D. Cates, J.-P. Chen, and Z.-E. Meziani, Spokespersons,
and
the E94-010 Collaboration.

E94-010 took data on the inclusive scattering of polarized electrons from polarized ^{3}He thus providing some of the first detailed information on the spin structure of ^{3}He at low Q^2. A central goal of the experiment is the study of the extended Gerasimov-Drell-Hearn (GDH) sum rule. The data analysis is nearly complete, and preliminary results on the Q^2-dependence of the GDH sum have been presented at several conferences. Results have also been presented on spin asymmetries, absolute cross sections, and the spin structure functions $g_1(x, Q^2)$ and $g_2(x, Q^2)$.

The original GDH sum rule relates the spin-dependent photoabsorption cross sections to the square of the anomalous magnetic moment of the object off which one is scattering. While the GDH sum rule involves the scattering of real photons, corresponding to $Q^2 = 0$, it is natural to consider the scattering of virtual photons where $Q^2 \neq 0$. It has been recognized for some time that it is possible to define a sum that is constrained by the GDH sum rule at $Q^2 = 0$, and by high energy data on spin structure for $Q^2 >> 1\,\mathrm{GeV}^2$. Recently, however, Ji and Osborne were able to define a rigorous new sum rule that relates the spin structure function $g_1(x, Q^2)$ to the forward virtual Compton scattering amplitudes [36]. This sum rule, which is well defined at all values of Q^2, reduces to the GDH sum rule at $Q^2 = 0$, and reproduces high energy results such as the Bjorken Sum Rule at $Q^2 >> 1\,\mathrm{GeV}^2$. With the extended GDH sum rule, one has an experimentally accessible observable that can be studied from a regime that is best described with quark degrees of freedom, to a regime that is best described with hadronic degrees of freedom. Many theoretical results exist with which to compare our results. Near $Q^2 = 0$, one can use Chiral perturbation theory [37,38]. At large values of Q^2, the GDH sum can be predicted using a twist expansion (with constraints from experimental data) [39,40]. In the intermediate range of Q^2, it may be necessary to use lattice gauge theory to arrive at accurate predictions. We note also that phenomenological models make predictions for the GDH sum [41]. The study of the extended GDH sum rule thus provides an excellent opportunity to study the dynamics of the strong interaction.

Data were collected at six energies (862, 1720, 2591, 3384, 4240, and 5070 MeV) and numerous spectrometer settings, all at a scattering angle of 15.5°. In energy loss, we had kinematic coverage from the quasielastic peak to the beginning of the deep inelastic regime. In Q^2, our data are sufficient to make meaningful statements about the GDH integral over the range $0.1\,\mathrm{GeV}^2 \leq Q^2 \leq 1.0\,\mathrm{GeV}^2$.

Because we were studying inclusive scattering, both of the Hall A spectrometers were used to detect electrons. A shower counter was built and installed in the Hadron Arm to aid in pion rejection. During some of our running, two DAQ systems were used (one for each arm) permitting data acquisition rates as high as 5 kBytes/sec. Polarized electrons were provided by a strained GaAs cathode, yielding polarizations of roughly 70%.

A major technical achievement of our experiment was a concentrated effort by our collaboration to build and commission the Hall A polarized ^{3}He target (see section 1.9), which has the highest figure of merit in terms of thickness and polarization that has ever been achieved for a target of its type. The target length was 40 cm, and the density corresponded to 10–12 atmospheres. Despite beam currents as high as 15 μA, the target polarization was maintained at 32–40% throughout most of our data taking. Somewhat higher polarizations were possible when using lower beam currents. Two separate methods were used to calibrate the polarization of the target that agreed well within errors, and resulted in a polarimetry error of 4.0%. The target polarization was also checked against the asymmetries observed in elastic scattering, and again good agreement was seen.

Because we are measuring absolute cross sections, we spent considerable effort understanding the spectrometer optics. For this purpose, we used some of our beam time to acquire what at the time was the most complete set of optics data to date by scattering off seven carefully spaced carbon foils. The seven foils were important to understand our ^{3}He target which is quite extended in length. We used our optics data to refine a monte carlo simulation so that we would have a good understanding of our acceptance for all of our many kinematic points.

We have completed all major phases of the data analysis, and are now in the process of checking and refining our results. In the analysis of our raw data, we have studied many issues, including scintillator efficiencies, Čerenkov efficiencies, dead-time corrections, and shower counter calibrations.

With our raw asymmetries and cross sections in hand, we applied radiative corrections using a modified version of the program POLRAD. We also accounted for dilution due to small amounts of N_2 in our target. We thus extracted both spin-averaged and spin-dependent cross sections for the six energies we studied. These results can be used to extract $g_1(x, Q^2)$ and $g_2(x, Q^2)$ over the same ranges.

The extended GDH sum rule involves evaluating the GDH sum at constant Q^2. To do this, we must extract g_1 and g_2 at constant Q^2 from our measured quantities. Over most of the kinematic range of interest, we are able to do this by interpolating between our actual measured points. We have accordingly constructed values for g_1 and g_2 at ten values of Q^2 ranging from $0.1\,\mathrm{GeV}^2$ to $1.0\,\mathrm{GeV}^2$. From these data, we can compute the GDH sum.

We are currently preparing a manuscript describing our results while we check and finalize our analysis. We expect to submit this manuscript for publication in early 2001. We note finally that two students have received Ph.D.'s for work related to E94-010, and that three more expect to receive Ph.D.'s shortly.

4 References

References

[1] http://www.jlab.org/e94010/

[2] JLab E94-010, Spokespersons, Z. E. Meziani, G. Cates and J. P. Chen.

[3] W. Xu, *et al.*, Phys. Rev. Lett. **85**, 2900 (2000).

[4] J. S. Jensen, Ph.D. Thesis, California Institute of Technology, 2000 (unpublished); I. Kominis, presentation at the E94-010 collaboration meeting, Sept., 2000

[5] http://hallaweb.jlab.org/equipment/targets/cryotargets/

[6] http://www.calstatela.edu/academic/nuclear_physics/89044/Iscan.htm

[7] René Brun and Fons Rademakers, "ROOT — An Object-Oriented Data Analysis Framework", Proceedings AIHENP'96 Workshop, Lausanne, Sep. 1996, Nucl. Instrum. Methods Phys. Res. A**389**, 81 (1997).

[8] The ROOT System Web site: `http://root.cern.ch`.

[9] L. Bimbot *et al.*, in preparation.

[10] M.W. McNaughton *et al.*, Nucl. Instrum. Methods Phys. Res. A **241**, 435 (1985).

[11] B. Bonin *et al.*, Nucl. Instrun. Methods A**A288**, 379 (1990).

[12] I.R. Afnan *et al.*, nucl-th/0006003, accepted for publication in Phys. Rev. C.

[13] Z. E. Meziani, Proceedings of the HiX2000 workshop, J.P. Chen and Z.E. Meziani, editors.

[14] http://www.jlab.org/div_dept/physics_division/GeV/HallA.12GeV.ps

[15] M. K. Jones *et al.*, Phys. Rev. Lett. **84**, 1398 (2000).

[16] B. Milbrath *et al.*, Phys. Rev. Lett. **80**, 452 (1998); erratum, Phys. Rev. Lett. **82**, 2221 (1999).

[17] K. Aniol *et al.*, Phys. Rev. Lett. 82 (1999) 1096.

[18] B. Mueller *et al.*, Phys. Rev. Lett. 78 (1997) 3824.

[19] D. T. Spayde *et al.*, Phys. Rev. Lett. 84 (2000) 1106.

[20] M. J. Musolf *et al.,* Phys. Rep. **239**, 1 (1994) and references therein.

[21] M. J. Musolf and B. R. Holstein, Phys. Lett. B 242 (1990) 461.

[22] S.-L Zhu *et al.,* preprint hep-ph/0002252.

[23] R. Hasty, accepted for publication in *Science*, 2000.

[24] Particle Data Group, C. Caso *et al.,* Eur. Phys. J. C 3 (1998) 1. The electroweak radiative corrections are essentially the same as for atoms. In addition, the peaking approximation is used to correct for the radiative tail.

[25] N. Isgur, G. Karl, and R. Koniuk, Phys. Rev. D **25**, 2394 (1982).

[26] A.J. Buchmann, hep-ph/9909385.

[27] M. Fiolhais, B. Golli, and S. Sirca, Phys. Lett. B**373**, 229 (1996).

[28] S.S. Kamalov and S.N. Yang, Phys. Rev. Lett. **83**, 4494 (1999).

[29] D.H. Lu, K. Tsushima, A.W. Thomas, A.G. Williams and K. Saito, Phys. Lett. B**417**, 217 (1998) and Phys. Rev. C **60** 068201 (1999).

[30] M.R. Frank, B.K. Jennings and G.A. Miller, Phys. Rev. C **54**, 920 (1996).

[31] P. A. Guichon, G. Q. Liu and A. W. Thomas, Nucl. Phys. A**591**, 606 (1995); P.A. Guichon, and M. Vanderhaeghen Prog. Part. Nucl. Phys. **41**, 125 (1998).

[32] E93-050 web page: http://www.jlab.org/~luminita/vcs.html

[33] VCSSIM code, L. Hoorebeke, Gent Univ.

[34] M. Vanderhaeghen *et al.*, Phys. Rev. C**62**, 025501 (2000)

[35] D. Drechsel *et al.*, Nucl Phys A**645** (1999) 145, and http://www.kph.uni-mainz.de/MAID/

[36] Xiangdong Ji and Jonathan Osborne, hep-ph/9905410.

[37] X. Ji, C. Kao and J. Osborne, Phys. Lett. B**472**, 1 (2000).

[38] V. Bernard, N. Kaiser and U.-G. Meissner, Phys. Rev. D**48**, 3062 (1993).

[39] X. Ji and P. Unrau, Phys. Rev. D**52**, 72 (1995).

[40] X. Ji and W. Melnitchouk, Phys. Rev. D**56**, 5511 (1997).

[41] D. Drechsel, S.S. Kamalov, and L. Tiator, hep-ph/0008306.

5 Members of the Hall A Collaboration

Bryon Anderson	Kent State University
Konrad A. Aniol	Cal State University
John Annand	University of Glasgow
David S. Armstrong	College of William and Mary
Todd Averett	College of William and Mary
Maud Baylac	DAPNIA/SPhN, CEA, Saclay
Elizabeth Beise	University of Maryland
Fatiha Benmokhtar	Rutgers University
J. Berthot	Universit Blaise Pascal, Clermont-Ferrand
Pierre Bertin	Universit Blaise Pascal, Clermont-Ferrand
Bill Bertozzi	MIT
Louis Bimbot	Institut de Physique Nucleaire, Orsay
Tim Black	MIT
Werner Boeglin	Florida International University
Ed Brash	University of Regina
Vincent Breton	Universit Blaise Pascal, Clermont-Ferrand
Herbert Breuer	University of Maryland
David Brown	University of Maryland
Etienne Burtin	DAPNIA/SPhN, CEA, Saclay
John Calarco	University of New Hampshire
Larry Cardman	Jefferson Lab
Gordon D. Cates	University of Virginia
Christian Cavata	DAPNIA/SPhN, CEA, Saclay
Zengwei Chai	MIT
George Chang	University of Maryland
Ting Chang	University of Illinois
Nicholas Chant	University of Maryland
Jian-Ping Chen	Jefferson Lab
Seonho Choi	Temple University
Eugene Chudakov	Jefferson Lab
Steve Churchwell	Duke University
Evaristo Cisbani	INFN/Sezione Sanita

Nathalie Colombel	DAPNIA/SPhN, CEA, Saclay
Marius Coman	Florida International University
Dan Dale	University of Kentucky
Natalie Degrande	Gent State University
Kees de Jager	Jefferson Lab
Raffaele De Leo	INFN/Sezione Bari
Alexandre Deur	University of Virginia
Nicole d'Hose	DAPNIA/SPhN, CEA, Saclay
Sonja Dieterich	Rutgers University
Rachele di Salvo	Universit Blaise Pascal, Clermont-Ferrand
Pibero Djawotho	College of William and Mary
Jean-Eric Ducret	DAPNIA/SPhN, CEA, Saclay
Dipangkar Dutta	MIT
Kim Egiyan	Yerevan Physics Institute
Martin B. Epstein	Cal State University
Stephanie Escoffier	DAPNIA/SPhN, CEA, Saclay
Mike Finn	College of William and Mary
Kevin Fissum	University of Lund
Helene Fonvieille	Universit Blaise Pascal, Clermont-Ferrand
Bernard Frois	DAPNIA/SPhN, CEA, Saclay
Salvatore Frullani	INFN/Sezione Sanita
Haiyan Gao	MIT
Franco Garibaldi	INFN/Sezione Sanita
Ashot Gasparian	Hampton University
Olivier Gayou	College of William and Mary
Shalev Gilad	MIT
Ron Gilman	Rutgers University
Alexander Glamazdin	Kharkov Institute of Physics and Technology
Charles Glashausser	Rutgers University
Javier Gomez	Jefferson Lab
Victor Gorbenko	Kharkov Institute of Physics and Technology
Tim Gorringe	University of Kentucky
Keith Griffioen	College of William and Mary
Ole Hansen	Jefferson Lab
Bill Hersman	University of New Hampshire
Doug Higinbotham	MIT
Richard Holmes	Syracuse University
Harry Holmgren	University of Maryland
Maurik Holtrop	University of New Hampshire

Edik Hovhannisyan	Yerevan Physics Institute
Calvin Howell	Duke University
Garth Huber	University of Regina
Charles Hyde-Wright	Old Dominion University
Sebastian Incerti	Temple University
Mauro Iodice	INFN/Sezione Sanita
Riccardo Iommi	INFN/Sezione Sanita
Dave Ireland	University of Glasgow
Stephanie Jaminion	Universit Blaise Pascal, Clermont-Ferrand
Steffen Jensen	Cal Tech
Xiangdong Jiang	Rutgers University
Cathleen Jones	Cal Tech
Mark K. Jones	University of Maryland
Christophe Jutier	Universit Blaise Pascal, Clermont-Ferrand
Seigo Kato	Yamagata University
Mina Katramatou	Kent State University
James Kellie	University of Glasgow
James Kelly	University of Maryland
Sophie Kerhoas	DAPNIA/SPhN, CEA, Saclay
Armen Ketikyan	Yerevan Physics Institute
Kouichi Kino	Tohoku University
Ioannis Kominis	Princeton University
Wolfgang Korsch	University of Kentucky
Serge Kox	Institut des Sciences Nuclaires, Grenoble
Kevin Kramer	College of William and Mary
Laird Kramer	Florida International University
Krishna S. Kumar	University of Massachusetts
Gerfried Kumbartzki	Rutgers University
Michael Kuss	Jefferson Lab
Geraud Lavessiere	Universit Blaise Pascal, Clermont-Ferrand
John LeRose	Jefferson Lab
Mark Leuschner	University of New Hampshire
David Lhuillier	DAPNIA/SPhN, CEA, Saclay
Richard Lindgren	University of Virginia
Ken Livingston	University of Glasgow
Nilanga Liyanage	Jefferson Lab
George Lolos	University of Regina
Robert Lourie	Renaissance Technology

Richard Madey	Kent State University
Kazushige Maeda	Tohoku University
Mark Manley	Kent State University
Demetrius Margaziotis	Cal State University
Pete Markowitz	Florida International University
Jacques Marroncle	DAPNIA/SPhN, CEA, Saclay
Jacques Martino	DAPNIA/SPhN, CEA, Saclay
Samvel Mayilyan	Yerevan Physics Institute
Kathy McCormick	Kent State University
David Meekins	Florida State University
Zein-Eddine Meziani	Temple University
Bob Michaels	Jefferson Lab
Brian Milbrath	University of Virginia
Wilson Miller	Princeton University
Joe Mitchell	Jefferson Lab
Jean Mougey	Institut des Sciences Nuclaires, Grenoble
Sirish Nanda	Jefferson Lab
Alan Nathan	University of Illinois
Damien Neyret	DAPNIA/SPhN, CEA, Saclay
Zisis Papandreou	University of Regina
Charles Perdrisat	College of William and Mary
Gerassimos G. Petratos	Kent State University
Artush Petrosyan	Yerevan Physics Institute
Stephane Platchkov	DAPNIA/SPhN, CEA, Saclay
Roman Pomatsalyuk	Kharkov Institute of Physics and Technology
Vina Punjabi	Norfolk State University
Thierry Pussieux	DAPNIA/SPhN, CEA, Saclay
Gilles Qumner	College of William and Mary
Ronald Ransome	Rutgers University
Brian Raue	Florida International University
Juerg Reinhold	Florida International University
Yves Roblin	Universit Blaise Pascal, Clermont-Ferrand
Rikki Roche	Florida State University
Mike Roedelbronn	University of Illinois
Oscar Rondon	University of Virginia
Philip Roos	University of Maryland
Guenther Rosner	University of Glasgow
David Rowntree	MIT
Gary Rutledge	College of William and Mary
Paul Rutt	Jefferson Lab

Marat Rvachev	MIT
Franck Sabatie	Old Dominion University
Arun Saha	Jefferson Lab
Teijiro Saito	Tohoku University
Adam J. Sarty	Saint Mary's University
Albert Shahinyan	Yerevan Physics Institute
Karl Slifer	Temple University
Timothy Smith	University of New Hampshire
Pavel Sorokin	Kharkov State University
Paul A. Souder	Syracuse University
Steffen Strauch	Rutgers University
Riad Suleiman	MIT
Jeff Templon	University of Georgia
Tatsuo Terasawa	Tohoku University
Luminita Todor	Old Dominion University
H. Tsubota	Tohoku University
Hiroaki Ueno	Yamagata University
Paul E. Ulmer	Old Dominion University
Guido Urciuoli	INFN/Sezione Sanita
Luc Van de Hoorebeke	Gent State University
Robert Van de Vyver	Gent State University
Pascal Vernin	DAPNIA/SPhN, CEA, Saclay
Branislav (Branko) Vlahovic	North Carolina Central University
Hakob Voskanyan	Yerevan Physics Institute
Eric Voutier	Institut des Sciences Nuclaires, Grenoble
Richard Walter	Duke University
John Watson	Kent State University
Dan Watts	University of Glasgow
Larry Weinstein	Old Dominion University
Richard Wilson	Harvard University
Krishni Wijesooriya	Argonne National Lab
Bogdan Wojtsekhowski	Jefferson Lab
Hong Xiang	MIT
Feng Xiong	MIT
Wang Xu	MIT
Valdis Zeps	University of Kentucky
Jianguo Zhao	General Electric
Xiaochao Zheng	MIT
Zilu Zhou	MIT
Liuyyan Zhu	MIT

6 Completed Hall A Experiments

Exp. #	Title	Spokespersons	Beam Days
	Nucleon and Meson Form Factors and Sum Rules		
E93-027	Electric Form Factor of the Proton by Recoil Polarization	C.F. Perdrisat V. Punjabi	16
E94-010	Measurement of the Neutron (^{3}He) Spin Structure Function at Low Q^2; a Connection between the Bjorken and D-H-G Sum Rules	G. Cates Z.-E. Meziani J.-P. Chen	31
E99-007	Measurement of $G^p{}_E/G^p{}_M$ to $Q^2 = 5.6\ GeV^2$ by the Recoil Polarization Method	C.F. Perdrisat M. Jones V. Punjabi E. Brash	28
	Few Body Nuclear Properties		
E89-019	Measurement of Proton Polarization in the $d(\gamma, p)n$ Reaction	R. Gilman R.J. Holt Z.-E. Meziani	18
E89-028	Polarization Transfer Measurements in the D(e,e'p)n Reaction	J.M. Finn M. Jones P.E. Ulmer	8
E89-044	Selected Studies of the ^{3}He and ^{4}He Nuclei Through Electrodisintegration at High Momentum Transfer	M. Epstein M. Kuss A. Saha E. Voutier	30
E91-026	Measurement of the Electric and Magnetic Structure Functions of the Deuteron at Large Momentum Transfers	G. Petratos J. Gomez	24
E93-049	Polarization Transfer in the Reaction $^4He(e, e'p)^3H$ in the Quasi-Elastic Scattering Region	R. Ent P.E. Ulmer	12

Exp. #	Title	Spokespersons	Beam Days
	Few Body Nuclear Properties (cont'd)		
E94-004	In-Plane Separation and High Momentum Structure in d(e,e'p) *(partially completed))*	P.E. Ulmer M. Jones	3
E95-001	Precise Measurements of the Inclusive Spin-dependent Quasi-Elastic Transverse Asymmetry A'_T at Low Q^2	H. Gao J.-O. Hansen	15
E99-008	Large-Angle Two-Body Photodisintegration of the Deuteron at High Energy *(concurrent with E89-019)*	R. Gilman R.J. Holt Z.-E. Meziani	0
	Properties of Nuclei		
E89-003	Study of the Quasi-elastic (e,e'p) Reaction in ^{16}O at High Recoil Momenta	W. Bertozzi R. Lourie A. Saha L. Weinstein	10
E89-033	Measurement of Recoil Polarization in the ^{16}O(e,e'p) Reaction with 4 GeV Electrons	C.C. Chang C. Glashausser S. Nanda	10
	N* and Meson Properties		
E91-011	Investigation of the $N \to \Delta$ Transition via Polarization Observables in Hall A	S. Frullani J.J. Kelly A.J. Sarty	45
E93-050	Nucleon Structure Study by Virtual Compton Scattering	P.Y. Bertin P. Guichon C. Hyde-Wright	10
E94-012	Measurement of Photoproton Polarization in the $H(\gamma,p)\pi^0$ Reaction	R. Gilman R.J. Holt	8
	Strange Quarks		
E91-010	Parity Violation in Elastic Scattering from the Proton and ^{4}He	J.M. Finn P. Souder	42

7 Hall A Publications

- Transverse Asymmetry A'_T from the quasielastic $^3\vec{H}e(\vec{e},e)$ process and Neutron Magnetic Form Factor, W. Xu *et al.*, Phys. Rev. Lett. **84,** 3265 (2000).

- Field mapping of the Hall A high-resolution spectrometers of the Thomas Jefferson National Accelerator Facility, P. Vernin *et al.*, Nucl. Instrum. Methods **A449,** 505 (2000).

- Dynamical Relativistic effects in Quasielastic 1p-Shell Proton knockout from ^{16}O, J. Gao *et al.*, Phys. Rev. Lett. **84,** 3265 (2000).

- Polarization transfer in the $^{16}O(\vec{e},e'\vec{p})$ reaction, S. Malov *et al.*, Phys. Rev. C **62**, 057302 (2000)

- G_{E_p}/G_{M_p} Ratio by polarization transfer in $\vec{e}p \rightarrow e\vec{p}$, M. K. Jones *et al.*, Phys. Rev. Lett. **84,** 1398 (2000).

- Measurement of the neutral weak form factors of the proton, K.A. Aniol *et al.,* Phys. Rev. Lett. **82,** 1096 (1999).

- Measurement of the Deuteron Elastic Structure Function $A(Q^2)$ at Jefferson laboratory, L. C. Alexia *et al.,* Phys. Rev. Lett. **82,** 1374 (1999).

- The CO_2 gas Cherenkov detectors for the Jefferson Lab Hall-A spectrometers, M. Iodice *et al.*, Nucl. Instrum. Methods **A411,** 223 (1998).